

Driftdfusion

An open source code for simulating ordered semiconductor devices with mixed ionic-electronic conducting materials in one-dimension

Philip Calado¹ · Ilario Gelmetti² · Benjamin Hilton¹ · Mohammed Azzouzi¹ · Jenny Nelson¹ · Piers R. F. Barnes¹

arXiv submission date: 9th September 2020

Abstract The recent emergence of lead-halide perovskites as active layer materials for thin film semiconductor devices including solar cells, light emitting diodes, and memristors has motivated the development of several new drift-diffusion models that include the effects of both mobile electronic and ionic charge carriers. The aim of this work is to provide a comprehensive guide to Driftdfusion, a versatile simulation tool built for modelling one-dimensional ordered semiconductor devices with mixed ionic-electronic conducting layers. Driftdfusion enables users to model devices with multiple, distinct, material layers using up to four charge carrier species: electrons and holes by default plus up to two ionic species. The time-dependent carrier continuity equations are fully-coupled to Poisson's equation enabling transient optoelectronic device measurement protocols to be simulated. In addition to material and device-wide properties, users have direct access to adapt the physical models for carrier transport, generation and recombination. Furthermore, a graded-interface approach circumvents the requirement for boundary conditions at material interfaces and enables interface-specific properties, such as high rates of interfacial recombination, to be introduced.

Keywords semiconductor device simulation · numerical modelling · drift-diffusion · solar cells · perovskites · ionic-electronic conductors · device physics

UK Engineering and Physical Sciences Research Council grant No. EP/J002305/1, EP/M025020/1, EP/M014797/1, EP/R020574/1, EP/R023581/1, and EP/L016702/1, European Unions Horizon 2020 research and innovation program grant agreement No. 742708.

P. Calado

E-mail: p.calado13@imperial.ac.uk

¹ Department of Physics, Imperial College London, London SW7 2AZ, UK.

² Institute of Chemical Research of Catalonia (ICIQ), Barcelona Institute of Science and Technology (BIST), Avda. Paisos Catalans 16, 43007 Tarragona, Spain.

1 Introduction

1.1 Drift-diffusion modelling

Accurate models of semiconductor devices are essential to further our understanding of the key physical processes governing these systems and hence rationally optimise them. One approach to modelling devices on the mesoscopic scale is to use continuum mechanics, whereby charge carriers are treated as continuous media as opposed to discrete particles. Typically, electronic carriers are modelled as electron and hole densities at discrete energy levels with a transport model describing the dynamics of carriers in response to an electric field (drift) and carrier density gradients (diffusion). This drift-diffusion (Poisson-Nernst-Planck) treatment leads to a system of coupled partial differential equations (the van Roosbroeck system[41, 17]): a set of continuity equations, defining how charge carrier densities change in time at each spatial location, are coupled with Poisson's equation (Gauss' Law), which relates the space-charge density to the electric field potential. For many architectures of thin-film semiconductor device, provided that the materials are homogeneous and isotropic, it is sufficient to model devices with properties that vary in a single spatial direction. In all but the most elementary of cases, these one-dimensional, second-order, coupled equations must be solved numerically.

1.2 The emergence of lead-halide perovskites and recent progress in mixed electronic-ionic conductor device models

The recent emergence of lead-halide perovskites (referred to herein as perovskites) as active layer materials for thin film semiconductor devices including solar cells, light emitting diodes (LEDs), and memristors has motivated the development of several new drift-diffusion models.[19, 30, 31, 27,

13, 4] Ab initio calculations and experimental evidence has shown that the space-charge, and consequently the electric field, in perovskite materials is dominated by slow-moving mobile ionic defects rather than electrons and holes under most conditions.[43, 16, 44, 20] This has a profound impact on the optoelectronic response of devices with perovskite active layers, leading to strong hysteresis effects in experimental measurements on timescales from microseconds to hundreds-of-seconds.[25, 10]

To date, both experimental and theoretical research into perovskites has primarily focussed on their application as a photovoltaic absorber material in solar cells and we now review the recent advances in device-level modelling for this application. Van Reenen, Kemerink & Snaith were the first to publish simulations using a coupled model that included continuity equations for three charge carriers: electrons, holes and a mobile ionic species.[30] They found that current-voltage (J - V) hysteresis in PSCs could only be reproduced by including a density of trap states close to one of the interfaces acting as a recombination centre.[30] Later calculations of a 1.5 nm Debye length¹[31] suggested, however, that the choice of a 4 nm mesh spacing in the simulations was too coarse to properly resolve the ionic charge profiles at the interfaces (described herein as interfaces). Richardson and co-workers overcame the numerical challenge of high ionic carrier and potential gradients at the interfaces by using an asymptotic analytical model to calculate the potential drop in the Debye layers of a single mixed electronic-ionic conducting material layer.[19, 31] While this approach enabled the reproduction of hysteresis effects using high rates of bulk recombination, the inability to accurately model interfacial recombination limited the degree to which the simulation could represent real-world devices.[31] In a later publication by the same group modelling dark current transients, interfacial recombination was implemented, but only at the inner boundary of the Debye layer.[29] Furthermore, since these models were limited to a single layer, unrealistically large ionic charge densities were calculated at the interfaces as compared to three-layer models with discrete electron and hole transport layers (ETL and HTL respectively).

Our own simulation work began with a three-layer p-i-n dual homojunction model in which the p- and n-type regions simulated the HTL and ETL and where interfacial recombination was approximated by including high rates of recombination throughout these layers. Our results supported van Reenen et al.'s conclusion that both mobile ions and high rates of interfacial recombination are required to reproduce J - V hysteresis effects and other comparatively slow transient optoelectronic phenomena in p-i-n solar cells.[8] Shortly after Neukom et al. published a modelling study with similar conclusions.[27] They used the commer-

cial package SETFOS[18] to solve for electronic carriers in combination with a separate MATLAB code that solved for the ionic carrier distributions. More recently, Courtier et al. published results from a freely-available, fully-coupled, three-layer device model that included a single ionic charge carrying species and boundary conditions at the interfaces such that interfacial recombination could be included.[13] Only the majority carriers were calculated in the ETL and HTL, excluding the possibility of simulating intrinsic or low-doped transport layers such as organic semiconductors. Furthermore, the doping densities in these regions were chosen to be the effective density of states, invalidating the use of Boltzmann statistics, a flaw that has since been corrected in the most recent release of the code.[14] Jacobs et al. also recently published results from a three-layer coupled electronic-ionic carrier simulation implemented using COMSOL Multiphysics®[11] and MATLAB Livelink™.[38][21] While their results included interfacial recombination, at the time of writing this code is not publicly available and the details of the methodology are sparse.

1.3 Driftfusion: An open source code for simulating ordered semiconductor devices with mixed ionic-electronic conducting materials in one-dimension

Here we present a comprehensive user guide to Driftfusion, our open source simulation tool designed for simulating semiconductor devices with mixed ionic-electronic conducting layers. The software enables users to simulate devices with multiple distinct material layers and up to four charge carrying species: electrons and holes by default plus up to two ionic species. The time-dependent continuity equations are fully-coupled to Poisson's equation enabling transient optoelectronic measurements to be simulated. In addition to material parameters, users have direct access to adapt carrier transport, recombination and generation models as well as the systems initial and boundary conditions. To model the mixing of states at material interfaces,[15] Driftfusion uses a graded interface approach for heterojunctions such that there is a smooth transition between the properties of adjacent layers. This method has the added benefits that it circumvents the requirement for additional system boundary conditions and enables interface-specific properties (such as high rates of interfacial recombination) to be defined within the graded regions. While the example architectures and outputs given in this work use PSCs as a model system, Driftfusion can, in principle, be used to model any non-degenerate one-dimensional mixed ionic-electronic semiconductor or redox system for which Boltzmann statistics provide a good approximation for the electronic carrier distribution function.

¹Based on an ion density of $1.6 \times 10^{19} \text{ cm}^{-3}$.

This report is divided into four main sections; We begin with a general overview of the simulation tool in Section 2; In Section 3 the default physical models for charge carrier transport, generation and recombination are outlined; In Section 4 calculations from Driftdiffusion are compared to two analytical and two numerical models to validate the solutions and the graded-properties interface approach; We conclude in Section 5 with a detailed description of the system architecture and a step-by-step guide of the important commands and functions that will enable the reader to get started using Driftdiffusion.

2 General overview of Driftdiffusion

2.1 Work flow

A flow diagram summarising Driftdiffusion's general work flow is given in Figure 1. The system is designed such that the user performs a linear series of steps to obtain a solution; (1) The user begins by creating a semiconductor device by defining both device-wide properties such as the carrier extraction coefficients, and layer specific properties such as the electronic band gap of each layer. A user-definable physical model comprised of generation, recombination and transport models is used to define the continuity equation for each charge carrier (see Section 3, Equations 26 - 29 for the default expressions); (2) The system of continuity equations are solved simultaneously with Poisson's equation (Equation 16) to obtain a solution for the electron density, hole density, cation density (optional), anion density (optional), and electrostatic potential spatial profiles (distributions) for the device equilibrium state; (3) An experimental protocol such as a current-voltage scan is defined with the appropriate input parameters e.g. the scan rate and limiting voltages. The protocol generates time-dependent voltage and light conditions that are applied to the device, typically using the equilibrium solution as the initial conditions. In more sophisticated protocols the solution is broken into a number of steps with intermediate solutions being fed back into the solver. Protocols can also be cascaded such that the solution from one protocol supplies the initial conditions for the next; (4) The final solution is output as a MATLAB structure comprised of the device properties, time and spatial meshes, and a solution matrix containing the electron density, hole density, cation density (optional), anion density (optional), and electrostatic potential spatial profiles (distributions) as a function of time (see *Solution structure* box); (5) The solution can be analysed to obtain calculated outputs such as the charge carrier currents, quasi-Fermi levels etc; (6) A multitude of plotting tools are also available to the user to visualise the solution and calculated outputs. Instructions on how to run each step programmatically and further details of

the system architecture, protocols, solutions, and analysis functions are given in Section 5.

2.2 Licensing information

The front end code of Driftdiffusion has been made open-source under the GNU General Public License v3.0 in order to accelerate the rate of development of perovskite and other mixed ionic-electronic conducting material-based technologies.[9] It is important to note, however, that Driftdiffusion presently uses MATLAB's Partial Differential Equation solver for Parabolic and Elliptic equations (pdepe), licensed under the MathWorks, Inc. Software License Agreement, which strictly prohibits modification and distribution. If you use Driftdiffusion please consider giving back to the project by providing feedback or contributing to its continued development and dissemination.

We now proceed by describing the default physical models underlying this release of Driftdiffusion. In the following description of the model relevant functions and scripts used in Driftdiffusion are highlighted using boxes and referred to using the MATLAB command line typeface.

Solution structures Following successful completion of the steps given in Figure 1, Driftdiffusion outputs a MATLAB structure `sol` (known herein as a *solution structure*) containing the following elements:

- The solution matrix `u`: a three-dimensional matrix for which the dimensions are [time, space, variable]. The order of the variables are as follows:
 1. Electrostatic potential
 2. Electron density
 3. Hole density
 4. Cation density (where 1 mobile ionic carrier is stipulated)
 5. Anion density (where 2 mobile ionic carriers are stipulated)
- The spatial mesh `x`.
- The time mesh `t`.
- The parameters object `par`.

As illustrated in Section 2.2, `sol` can be used as the input argument for analysis functions contained within `dfana` or plotting functions within `dfplot`. See Section 5 for further details.

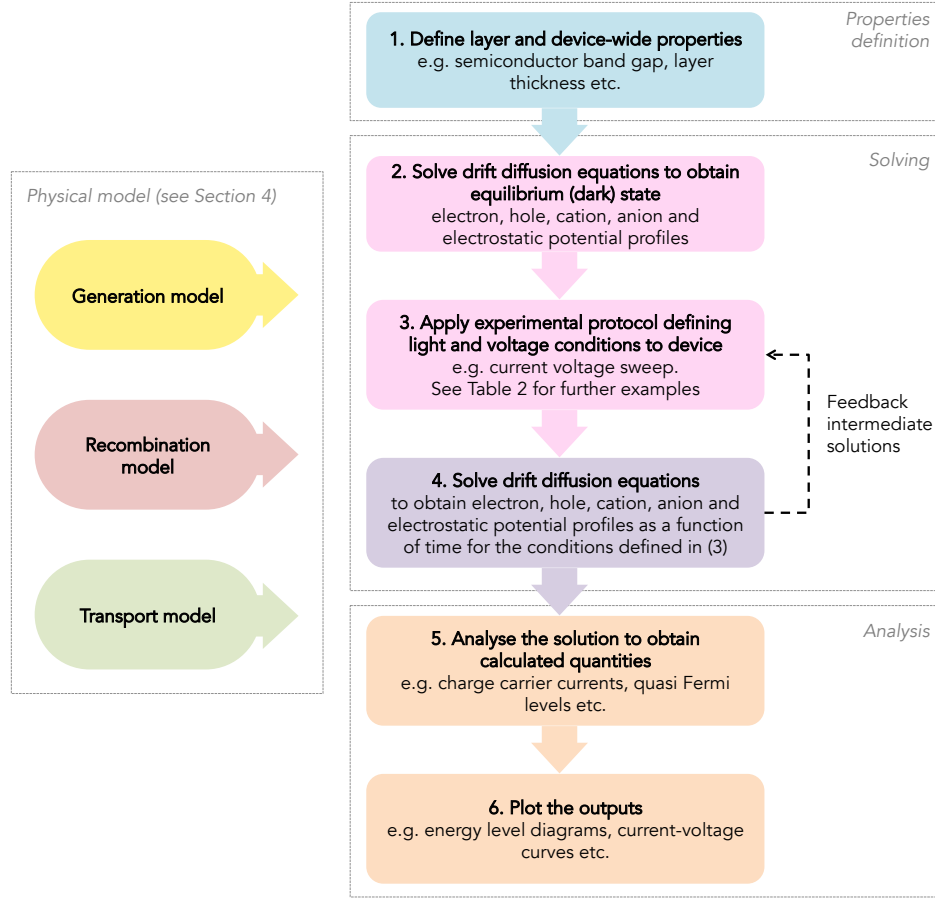


Fig. 1 The general workflow of Driftfusion. 1. The user defines a device in the properties definition step; 2. The device equilibrium state is solved for using the given recombination and transport models; 3. The user selects and runs an experimental protocol which defines time-dependent voltage and light conditions (derived from the appropriate generation model) to be applied to the equilibrium solution; 4. A solution is obtained that may be fed back into the protocol until a final solution is reached; 5. The solution is analysed to obtain calculated outputs; 6. The outputs are visualised using plotting tools.

3 Implementation of established semiconductor theoretical principles in Driftfusion

The device physics implemented in Driftfusion is principally based on established semi-classical semiconductor transport and continuity principles, which are well described in Sze & Kwok[37] and Nelson[26]. Large elements of this section are adapted from Ref. [7] and are provided here as a direct reference for the reader.

Driftfusion evolved from a diffusion-only code written to simulate transient processes in dye sensitised solar cells[2] and uses MATLAB's[38] built-in (pdepe) solver.[32] The code solves the continuity equations and Poissons equation for electron density n , hole density p , cation density c (optional), anion a (optional), and the electrostatic potential V as a function of position x , and time t . The full details of the numerical methods employed by the pdepe

solver for discretising the equations are given in Skeel & Berlins 1990.[35]

3.1 Semiconductor energy levels

Figure 2a shows the energy levels associated with an idealised intrinsic semiconductor. The electron affinity Φ_{EA} and ionisation potential Φ_{IP} are the energies released when an electron is added from the the vacuum level E_{vac} to the conduction band (CB) and valence band (VB) respectively.

The electronic band gap E_g of the material can be defined as:

$$E_g = \Phi_{EA} - \Phi_{IP} \quad (1)$$

The equilibrium Fermi energy E_{F0} defines the energy at which a hypothetical electronic state has a 50% probabil-

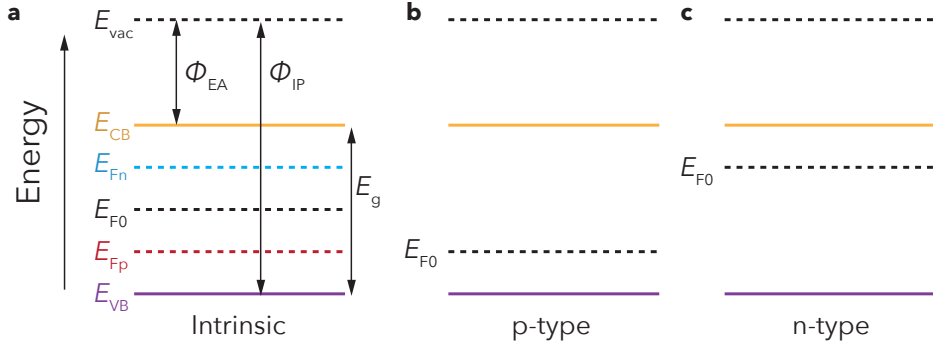


Fig. 2 Semiconductor energy levels. (a) An intrinsic semiconductor material showing the vacuum level E_{vac} , electron affinity Φ_{EA} , ionisation potential Φ_{IP} , conduction and valence band energies E_{CB} and E_{VB} , band gap E_g , intrinsic Fermi energy E_i and electron and hole quasi-Fermi levels E_{Fn} and E_{Fp} . (b) A p-type material: The equilibrium Fermi energy E_{F0} lies closer to the VB due to acceptor impurities adding holes to the VB. (c) An n-type material: E_{F0} lies closer to the CB as donor impurities increase the equilibrium CB electron density.

ity of occupation for intrinsic and doped semiconductors respectively. At equilibrium, and in the absence of an electric field, the Fermi energy is identical to the chemical potential. While for an idealised, defect-free semiconductor no states exists in within the band gap, for an intrinsic semiconductor, E_{F0} lies close to the middle of the gap. Where the semiconductor is p-type, dopant impurities accept electrons from the bands, shifting the equilibrium Fermi level E_{F0} towards the VB (Figure 2b). Similarly, where the semiconductor is n-type, dopants donate electrons to the bands, shifting E_{F0} towards the CB (Figure 2c). Below follows a brief description of how these energies are calculated in the simulation.

3.1.1 The vacuum energy

The vacuum energy, E_{vac} is defined as the energy at which an electron is free of all forces from a solid including atomic and external potentials.[26] Spatial changes in the electrostatic potential V are therefore reflected in E_{vac} such that, at any point in space,

$$E_{vac} = -qV, \quad (2)$$

where q is the elementary charge.

3.1.2 Conduction and valence band energies

The conduction and valence band energies E_{CB} and E_{VB} are defined as the difference between the vacuum energy and Φ_{EA} and Φ_{IP} respectively.

$$E_{CB} = -qV - \Phi_{EA} = E_{vac} - \Phi_{EA}, \quad (3)$$

$$E_{VB} = -qV - \Phi_{IP} = E_{vac} - \Phi_{IP}. \quad (4)$$

The band energies then, include both the potential energy owing to the specific molecular orbitals of the solid and the electrostatic potential arising from space charge accumulation both internal and external to the material.

3.2 Electronic carrier densities and quasi-Fermi levels

3.2.1 Equilibrium carrier densities

At equilibrium the net exchange of mass and energy into and out of the system is zero. Using the Boltzmann approximation to the Fermi-Dirac probability distribution function, the equilibrium electron and hole densities, n_0 and p_0 can be expressed as:

$$n_0 = N_{CB}(T) \exp\left(\frac{E_{F0} - (-\Phi_{EA})}{k_B T}\right) \quad (5)$$

$$p_0 = N_{VB}(T) \exp\left(\frac{(-\Phi_{IP}) - E_{F0}}{k_B T}\right), \quad (6)$$

where k_B is Boltzmann's constant, T is the temperature of the material and N_{CB} and N_{VB} are the temperature-dependent effective density of states (eDOS) of the conduction and valence bands respectively. For ordered semiconductors, close to the band edges, the electronic density of energy states (DOS) is typically approximated as a parabolic function with respect to crystal momentum and electron energy.

In charge-neutral n-type materials the equilibrium electron density is approximately equal to the density of dopant atoms, N_D such that

$$E_{F0} \approx -\Phi_{EA} + k_B T \ln\left(\frac{N_D}{N_{CB}}\right). \quad (7)$$

Similarly in p-type materials, $p_0 \approx N_A$, where N_A is the density of acceptor dopants, leading to the analogous expression

$$E_{F0} \approx -\Phi_{IP} - k_B T \ln \left(\frac{N_A}{N_{VB}} \right). \quad (8)$$

In Driftdiffusion users input values for E_{F0} for each material layer and the corresponding equilibrium carrier densities and doping densities are calculated when the user creates a parameters object (see Section 5.2) according to Equations 5 - 8.

The equilibrium carrier densities n_0 and p_0 and Fermi levels E_0 are calculated and stored as a function of position in the device structures `dev` and `dev_half` of the device parameters object `par`. See Subsection 5.2.4 for further details.

3.2.2 Quasi-Fermi levels

One of the key approximations in semiconductor physics is the assumption that, under external optical or electrical bias, the electron and hole populations at a particular location can be treated separately with individual distribution functions and associated quasi-Fermi levels (QFLs), E_{Fn} and E_{Fp} . This is permitted because thermal relaxation of carriers to the band edges is significantly faster than inter-band relaxation.[26] The QFLs can be described in terms of the electrochemical potential for the different carriers at each location:

$$E_{Fn}(x, t) = E_{CB}(V(x, t)) + k_B T \ln \left(\frac{n(x, t)}{N_{CB}(x)} \right) \quad (9)$$

$$E_{Fp}(x, t) = E_{VB}(V(x, t)) - k_B T \ln \left(\frac{p(x, t)}{N_{VB}(x)} \right) \quad (10)$$

The gradient of the QFLs provides a convenient way to determine the direction of the current since, from the perspective of the electron energy scale, electrons move ‘downhill’, and holes move ‘uphill’ in response to electrochemical potential gradients. Moreover, electron and hole currents, J_n and J_p , can be expressed in terms of the product of the QFL gradients with the electron and hole conductivities, σ_n and σ_p :

$$J_n(x, t) = \frac{\sigma_n}{q} \frac{dE_{Fn}(x, t)}{dx} \quad (11)$$

$$J_p(x, t) = \frac{\sigma_p}{q} \frac{dE_{Fp}(x, t)}{dx}, \quad (12)$$

Here, the conductivities are the product of the electronic carrier mobilities μ_n and μ_p with their corresponding concentrations and charge:

$$\sigma_n(x, t) = qn(x, t)\mu_n(x) \quad (13)$$

$$\sigma_p(x, t) = qp(x, t)\mu_p(x). \quad (14)$$

Both the band energies E_{cb} and E_{vb} , and electron and hole QFLs E_{fn} and E_{fp} can be calculated from a Driftdiffusion solution structure, `sol` by using the syntax:

```
[Ecb, Evb, Efn, Efp] = dfana.QFLs(sol)
```

The energies are output as a two dimensional matrices for which the dimensions are `[time, space]`. Please refer to Table S.3 for a full list of Driftdiffusion variable names and their corresponding symbols. For further details on the `dfana.my_calculation` syntax used in this section see Section 5.7.

3.2.3 Open circuit voltage

The open circuit voltage, V_{OC} is the maximum energy per unit charge that can be extracted from an electrochemical cell for any given illumination intensity. The V_{OC} can be calculated using the difference in the electron QFL at the cathode (x_{cat}) and the hole QFL at the anode (x_{ano}) with the cell at open circuit.

$$qV_{OC}(t) = E_{Fn}(x = x_{cat}, t) - E_{Fp}(x = x_{ano}, t), \quad (15)$$

The open circuit voltage as a function of time can be calculated using the command

```
Voc = dfana.calcVQFL(sol_OC)
```

Here, `sol_OC` is a solution for the device at open circuit obtained either by applying $V_{app} = V_{OC}$ or approximated by setting R_s to a high value for example $1 \text{ M}\Omega$ using the `lightonRs` protocol (see Section 5.4 for further information on protocols).

3.3 Poisson's equation

Poisson's equation (Gauss's Law) relates the electrostatic potential to the space charge density ρ and the material dielectric constant ϵ_r via the Divergence Theorem. The space charge density is the sum of the mobile carrier and static charge densities at each spatial location. Doping is achieved via the inclusion of fixed charge density terms for donors N_D and acceptors N_A , which generate counter electronic charges at equilibrium due to the thermal generation (negative recombination) terms included in the recombination expressions (Section 3.9). In the default version of Driftdiffusion mobile ionic carriers are modelled as Schottky defects[42] in which each ion has an oppositely charged counterpart, maintaining overall ionic charge neutrality within the device (excluding dopant ions). The mobile cation density c is initially balanced by a uniform static density N_{cat} and the mobile anion density a is balanced by N_{ani} . For the one-dimensional system thus far described, Poisson's equation can be explicitly stated as

$$\frac{\partial V(x,t)^2}{\partial x^2} = -\frac{\rho(x,t)}{\epsilon_0 \epsilon_r(x)} = -\frac{q}{\epsilon_0 \epsilon_r(x)}(p(x,t) - n(x,t) + c(x,t) - a(x,t) + \dots N_A(x) - N_D(x) - N_{cat}(x) + N_{ani}(x)), \quad (16)$$

where ϵ_0 is permittivity of free space. We emphasise that p , n , c , and a represent mobile species, while N_A , N_D , N_{cat} , and N_{ani} are static/immobile charge densities. In the default version of Driftdiffusion each species is assumed to have a charge of $\pm q$ per carrier, although the expressions can easily be adapted for other redox states by multiplication with an integer. See Section 5.5.1 for further details of how to edit the underlying physical equations.

Terms can be added or removed from Poisson's equation by editing the `S.potential` term in the equation editor in `dfpde` subfunction of the core `df` code. See Subsection 5.5 and Listing 1 for further details.

The space charge density (net charge density) `rho` can be output from a Driftdiffusion solution structure `sol` using the command:

```
rho = dfana.calcrho(sol)
```

`rho` is output as a two dimensional matrix for which the dimensions are `[time, space]`.

3.4 Charge transport: Drift and diffusion

As the name suggests, the drift-diffusion (Poisson-Nernst-Planck) model assumes that charge transport is driven by two processes:

1. *Drift* arising from the electrostatic force on charges due to an electric field $F = -dV/dx$.
2. *Diffusion* arising from the tendency for carriers to move from regions of high to low concentration.

In one dimension the expressions for the flux density of electrons j_n , holes j_p , anions j_a , and cations j_c with mobility μ_z and diffusion coefficient D_z , where z describes a generic charge carrier, are given by:

$$j_n(x,t) = -\mu_n(x)n(x,t)F(x,t) - D_n(x)\frac{\partial n(x,t)}{\partial x} \quad (17)$$

$$j_p(x,t) = \mu_p(x)p(x,t)F(x,t) - D_p(x)\frac{\partial p(x,t)}{\partial x} \quad (18)$$

$$j_a(x,t) = -\mu_a(x)a(x,t)F(x,t) - D_a(x)\left(\frac{\partial a(x,t)}{\partial x} + \frac{a(x,t)}{a_{max}(x) - a(x,t)}\frac{\partial a(x,t)}{\partial x}\right) \quad (19)$$

$$j_c(x,t) = \mu_c(x)c(x,t)F(x,t) - D_c(x)\left(\frac{\partial c(x,t)}{\partial x} + \frac{c(x,t)}{c_{max}(x) - c(x,t)}\frac{\partial c(x,t)}{\partial x}\right) \quad (20)$$

In Equations 19 and 20, the last terms follow a model proposed by Kilic et al. which limits the ionic carrier densities by accounting for steric effects at high ionic densities.[22] Here, a_{max} and c_{max} denote the limiting anion and cation densities.

Figure 3 illustrates how the direction of electron and hole flux densities is determined from gradients in the electric potential and charge carrier densities. An analogous diagram can be drawn for mobile ionic species by substituting cations for holes and anions for electrons.

The electric field calculated from the gradient of the potential `FV` and by integrating the space-charge density `Frho` can be obtained from a Driftdiffusion solution structure `sol` using the syntax:

```
[FV, Frho] = dfana.calcF(sol)
```

`FV` and `Frho` are output as a two dimensional matrices for which the dimensions are `[time, space]`.

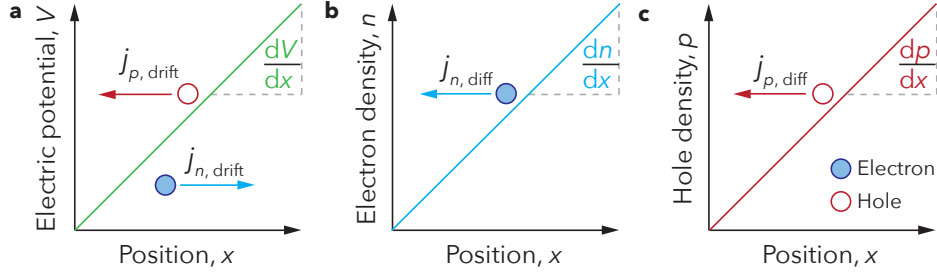


Fig. 3 Electron and hole carrier flux densities. Direction of electron j_n and hole j_p carrier flux densities in response to positive gradients in (a) the electric field potential (note: $F = -\frac{dV}{dx}$), and (b) electron and (c) hole carrier densities. The subscripts ‘drift’ and ‘diff’ denote drift and diffusion flux densities respectively. Analogous flux densities can be drawn for mobile ionic species by substituting cations for holes and anions for electrons.

3.4.1 Transport across heterojunction interfaces

Equations 17 and 18 can be modified by including additional gradient terms for spatial changes in Φ_{EA} , Φ_{IP} , N_{CB} , and N_{VB} to model interfacial regions between layers with differing material properties.[47] This leads to an adapted set of flux density equations for electrons and holes:

$$j_n(x,t) = \mu_n(x,t)n \left(-F(x,t) - \frac{\partial \Phi_{EA}(x)}{\partial x} \right) - D_n \left(\frac{\partial n(x,t)}{\partial x} - \frac{n(x,t)}{N_{CB}(x)} \frac{\partial N_{CB}(x)}{\partial x} \right) \quad (21)$$

$$j_p(x,t) = \mu_p(x,t)p \left(F(x,t) + \frac{\partial \Phi_{IP}(x)}{\partial x} \right) - D_p \left(\frac{\partial p(x,t)}{\partial x} - \frac{p(x,t)}{N_{VB}(x)} \frac{\partial N_{VB}(x)}{\partial x} \right) \quad (22)$$

A finite interface thickness must be used to allow discrete gradients to be specified for these properties.

The carrier (particle) currents are calculated as the product of the flux densities with the specific carrier charge such that $J_z = q_z j_z$.

The transport equations of Driftfusion can be edited using the carrier flux terms `F_electron`, `F_hole`, `F_cation`, and `F_anion` of the equation editor in the `dfpde` subfunction of the core `df` code. See Subsection 5.5 for further details.

$$J_{disp}(x,t) = -\epsilon_0 \epsilon_r(x) \frac{\partial F(x,t)}{\partial t}. \quad (23)$$

The negative sign included here accounts for the adopted current convention in Driftfusion: positive charges moving right and negative charges moving left constitute a positive current. While not directly calculated by the solver, the displacement current is an implicit component of the charge continuity equations.

3.4.3 Total current

The total current, J is the sum of the individual current components at each point in space and time:

$$J(x,t) = J_n(x,t) + J_p(x,t) + J_a(x,t) + J_c(x,t) + J_{disp}(x,t) \quad (24)$$

Fluxes and currents are calculated from the Driftfusion solution structure `sol` using the command:

```
[J, j, x] = dfana.calcJ(sol)
```

J is a structure containing the individual carrier particle currents `J.n`, `J.p`, `J.c`, and `J.a`, the displacement current `J.disp` and the total current `J.tot` at each spatial location and time calculated by integrating the continuity equations. j is a structure containing the corresponding carrier and total fluxes. x is the spatial grid upon which the fluxes and currents are calculated (see Subsection 3.10).

3.4.2 Displacement current

The displacement current J_{disp} , as prescribed in the Maxwell-Ampere law, is the rate of change of the electric displacement field, $\partial D / \partial t$. In terms of the electric field the displacement current can be expressed as

3.5 Charge continuity

The continuity equations are a set of ‘book keeping’ equations based on conservation of charge in the system. They

describe how charge carrier densities change as a function of time at each location. The continuity equation for a generic carrier density z with flux density j_z , and source/sink term S_z can be expressed as:

$$\frac{\partial z(x,t)}{\partial t} - \nabla j_z(x,t) - S_z(x,t) = 0. \quad (25)$$

For electronic carriers S_z is typically composed of two parts; 1. Generation g of carriers by thermal- or photo-excitation; 2. Recombination r of carriers through radiative (photon emission) and non-radiative pathways. Figure 4 illustrates the principle of continuity: changes in the electron concentration with time in a thin slab dx are determined by generation and recombination processes, and the difference between the incoming and outgoing flux density of particles.

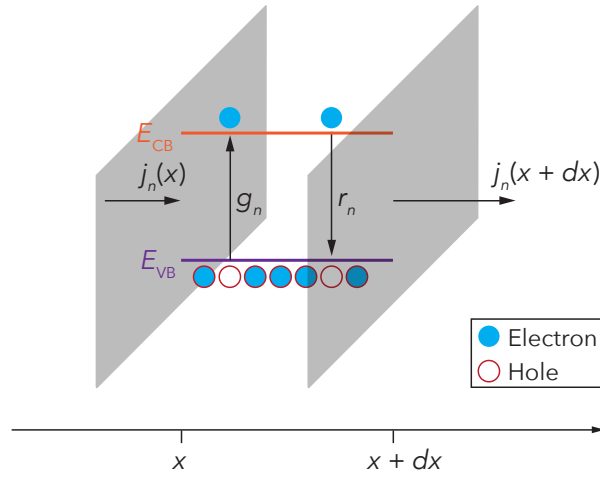


Fig. 4 Continuity of electronic charge in a one-dimensional system. Schematic illustrating the principle of continuity for electrons in a thin slab dx of material. A difference in the incoming and outgoing flux density j_n , generation g_n and recombination r_n of electrons result in changes in the electron concentration over dx . The conduction and valence bands are denoted E_{CB} and E_{VB} respectively. Figure concept taken from Ref.[46].

Where chemical reactions take place within devices, additional generation and recombination terms for carriers may also contribute to S . In the current version of Driftdiffusion, mobile ionic charge carriers are treated as inert species such that $g_c = g_a = r_c = r_a = 0$. Users are, however, free to edit the default source terms using the Equation Editor (Section 5.5). A guide describing how to do this is included in the Supplemental Information Section 5.

In one dimension the continuity equations for charge carriers are:

$$\frac{\partial n(x,t)}{\partial t} = -\frac{\partial j_n(x,t)}{\partial x} + g_n(x,t) - r_n(x,t) \quad (26)$$

$$\frac{\partial p(x,t)}{\partial t} = -\frac{\partial j_p(x,t)}{\partial x} + g_p(x,t) - r_p(x,t) \quad (27)$$

$$\frac{\partial a(x,t)}{\partial t} = -\frac{\partial j_a(x,t)}{\partial x} + g_a(x,t) - r_a(x,t) \quad (28)$$

$$\frac{\partial c(x,t)}{\partial t} = -\frac{\partial j_c(x,t)}{\partial x} + g_c(x,t) - r_c(x,t) \quad (29)$$

Equation 16 and Equations 26 - 29 form the complete set of coupled parabolic and elliptic equations to be solved numerically by pdepe.

3.6 Boundary conditions

Solving Equation 16 and Equations 26 - 29 requires two constants of integration for each variable, which are provided by the boundary conditions of the simulation. In Driftdiffusion a mix of Dirichlet (defined-variable value) and Neumann (defined-flux density value) boundary conditions are used; for the electronic carriers, Dirichlet conditions are used while Neumann conditions are used to fix the flux density of ionic carriers to zero at the boundaries under the assumption that ions are confined to the system, cannot be extracted and do not react at the boundaries. The electrostatic potential is fixed at both boundaries as detailed in Section 3.6.3. The details of these boundary conditions are set out in the following subsections.

The boundary conditions of the simulation can be edited in the `dfbc` subfunction of the core `df` code. See Subsection 5.5 for further details.

3.6.1 Electronic carrier contact selectivity and surface recombination

Many architectures of semiconductor device, including solar cells and LEDs employ selective contact layers that block minority carriers from being extracted (or injected) via energetic barriers. These are known variously as transport layers, blocking layers, blocking contacts, or selective contacts. In a solar cell for example, semiconductor layers are typically sandwiched between two metallic electrodes constituted of metals or highly-doped semiconductors such as indium tin oxide (ITO). Such materials are numerically challenging to simulate owing to their high charge carrier densities and thin depletion widths. Consequently, a common approach is to use boundary conditions defining charge carrier extraction and recombination flux densities to simulate the properties of either the contact or electrode material. It should be noted,

however, that the employment of fixed electrostatic potential boundary conditions (as defined in Section 3.6.3) implies that the potential falls only *within the discrete system* and not within the electrodes. This approach is only realistic for highly conductive electrode materials. Hence, to realistically simulate devices semiconductor contacts with lower conductivities, distinct electron and hole transport layers must be used.

For electronic carriers, rate coefficients s_n and s_p are used to define the rate of extraction of electrons and holes respectively, which for a good contact, is expected to be high (e.g. $> 10^7 \text{ cm s}^{-1}$). [39] For minority carriers, s_n and s_p are often described as *surface recombination velocity* coefficients, where low values simulate a highly selective contact and high values simulate a contact with poor selectivity. In Driftdusion the expressions for electronic boundary carrier flux densities, j_n and j_p are given by:

$$j_n(x=0, t) = s_{n,\text{left}}(n(x=0, t) - n_{\text{left}}) \quad (30)$$

$$j_p(x=0, t) = s_{p,\text{left}}(p(x=0, t) - p_{\text{left}}) \quad (31)$$

$$j_n(x=d, t) = s_{n,\text{right}}(n(x=d, t) - n_{\text{right}}) \quad (32)$$

$$j_p(x=d, t) = s_{p,\text{right}}(p(x=d, t) - p_{\text{right}}), \quad (33)$$

where n_{left} , n_{right} , p_{left} , and p_{right} are the equilibrium carrier densities at the left and right-hand boundaries, calculated using Equations 5 and 6, under the assumption that the semiconductor QFLs are at the same energy as the electrode workfunctions. For the left-hand boundary n_{left} and p_{left} are given by Equations 34 and 35.

$$n_{\text{left}} = N_{\text{CB}} \exp\left(\frac{\Phi_{\text{left}} - \Phi_{\text{EA}}}{k_B T}\right) \quad (34)$$

$$p_{\text{left}} = N_{\text{VB}} \exp\left(\frac{\Phi_{\text{IP}} - \Phi_{\text{left}}}{k_B T}\right) \quad (35)$$

Analogous expressions are used for n_{right} and p_{right} at the right-hand boundary. Extraction barriers can also be modelled with this approach by including a term for the barrier energy in the exponent of Equations 34 and 35. At the time of writing, quantum mechanical tunnelling and image charge density models for energetic barriers at the system boundaries are not included in Driftdusion.

3.6.2 Ionic carrier boundary conditions

In the simplest case, ionic carriers are confined to the device and do not react at the electrode boundaries. This leads to a set of zero flux density boundary conditions for mobile anions and cations:

$$j_a(x=0, t) = 0 \quad (36)$$

$$j_c(x=0, t) = 0 \quad (37)$$

$$j_a(x=d, t) = 0 \quad (38)$$

$$j_c(x=d, t) = 0 \quad (39)$$

Where an infinite reservoir of ions exists at a system boundary (such as an electrolyte), a Dirichlet boundary condition defining a constant ion density could alternatively be imposed.

The reader is referred to Section 5.5 for details on how to modify the boundary conditions of the simulation using the `dfbc` subfunction of the master `df` code.

3.6.3 Electrostatic potential boundary conditions

The built-in electrostatic potential V_{bi} of a semiconductor device is determined by the difference in boundary electrode workfunctions Φ_{left} and Φ_{right} :

$$qV_{\text{bi}} = \Phi_{\text{right}} - \Phi_{\text{left}} \quad (40)$$

For the default boundary conditions in Driftdusion the electrostatic potential at the left-hand boundary is set to zero (Equation 41) and used as the reference potential. The applied electrical bias, V_{app} and an effective potential arising from series resistance V_{R_s} are applied to the right-hand boundary as described in Equation 42.

$$V(x_0, t) = 0 \quad (41)$$

$$V(x_d, t) = V_{\text{bi}} - V_{\text{app}}(t) + V_{R_s}(t) \quad (42)$$

Here, we use Ohm's law is used to calculate V_{R_s} from the electron and hole flux densities:

$$V_{R_s}(t) = q(j_p(x=d, t) - j_n(x=d, t))R_s, \quad (43)$$

where R_s is the area-normalised series resistance, given by the product of the device series resistance and the device active area. It should be noted that the displacement current is omitted from this expression due to difficulty in calculating it dynamically at the boundary. Setting R_s to a high value (e.g. $R_s = 10^6 \Omega \text{ cm}^2$) approximates an open circuit condition for devices with metal electrodes. Technically this can be achieved using the `lighton_Rs` protocol (see Section 5.4 for a description of protocols). By contrast, setting $R_s = 0 \Omega \text{ cm}^2$ with $V_{\text{app}} = 0 \text{ V}$ simulates a short circuit condition.

The applied potential V_{app} as a function of time t can be reconstructed from a Driftfusion solution structure `sol` using the command:

```
Vapp = calcVapp(sol)
```

3.7 Initial conditions

The solver requires a set of initial conditions, one for each charge carrier variable and one for the electrostatic potential. In the current version of Driftfusion, two different sets of conditions are used dependent on the device type. The initial conditions are designed to be compatible with the boundary conditions and to minimise the error in space charge density at junctions which can lead to large electric fields and convergence failure.

The initial conditions of the simulation can be edited in the `dfic` subfunction of the core `df` code. See Subsection 5.5 for further details.

3.7.1 Single layer device

For a single layer device, a linearly varying electrostatic potential and exponentially varying electronic carrier densities over the layer thickness d are used for the initial conditions (Equations 44, 45, and 48). For the ionic carriers uniform densities are used throughout the layer to ensure charge neutrality (Equations 46 and 47).

$$n(x) = n_{\text{left}} \exp\left(\frac{x(\ln(n_{\text{right}}) - \ln(n_{\text{left}}))}{d}\right) \quad (44)$$

$$p(x) = p_{\text{left}} \exp\left(\frac{x(\ln(p_{\text{right}}) - \ln(p_{\text{left}}))}{d}\right) \quad (45)$$

$$a(x) = N_{\text{ani}}(x) \quad (46)$$

$$c(x) = N_{\text{cat}}(x) \quad (47)$$

$$V(x) = \frac{x}{d} V_{bi} \quad (48)$$

3.7.2 Multilayer device

For multilayer devices the electronic carrier densities are chosen to be the equilibrium densities for the individual layers (n_0 and p_0). As with the single layers, the ionic carriers are given a uniform density (Equations 49 - 52) and the electrostatic potential is set to fall uniformly throughout the device (Equation 53). While these initial conditions are inconsistent, they ensure that the boundary conditions are satisfied for the initial solution.

$$n(x) = n_0(x) \quad (49)$$

$$p(x) = p_0(x) \quad (50)$$

$$a(x) = N_{\text{ani}}(x) \quad (51)$$

$$c(x) = N_{\text{cat}}(x) \quad (52)$$

$$V(x) = \frac{x}{d_{\text{dev}}} V_{bi}, \quad (53)$$

where the device thickness d_{dev} is the sum of the individual layer thicknesses d_i ($d_{\text{dev}} = \sum_i d_i$). Driftfusion auto-detects the number of layers in the device and uses the appropriate set of initial conditions when running the `equilibrate` protocol to obtain the equilibrium solutions for the device (Section 5.3). The initial conditions are contained and can be edited in the `dfic` subfunction of the master `df` code (see Section 5.5).

3.8 Generation

Two optical models are currently available for use with Driftfusion, with options for up to two light sources (e.g. one bias and one excitation source). The generation profile is generated by the function `generation` during the call to the parameters class `pc` to create a parameters object (Section 5.2). The time-dependence of generation is determined by the function generator property settings (Section 5.5.5).

3.8.1 Uniform generation

A uniform volumetric generation rate, g_0 can be set for each layer using the `g0` property when creating the parameters object (see Section 5.2). By default the generation rate is set to zero in the interfaces. This avoids potential stability issues associated with high rates of generation and recombination at the same location.

3.8.2 Beer-Lambert law generation

The Beer-Lambert law models the photon flux density as falling exponentially with penetration distance and with a characteristic absorption coefficient α_{abs} . Over a range of photon energies E_γ , and for an incident photon flux density ϕ_0 , the volumetric generation rate g is given by the integral across the spectrum:

$$g(x) = (1 - \kappa) \int_0^\infty \alpha_{\text{abs}}(E_\gamma, x) \phi_0(E_\gamma) \exp(-\alpha_{\text{abs}}(E_\gamma, x)x) dE_\gamma, \quad (54)$$

where κ is the reflectance. For simplicity, we assume that a single electron-hole pair is generated by a single photon. Similar to uniform generation, carrier generation is set to zero in the interfaces to maintain code stability.

3.8.3 Arbitrary generation profile

An arbitrary generation profile can be inserted following creation of the parameters object for users who wish to use profiles calculated from different models using an external software package. Details on how to do this are given in Section 5.2.6.

3.9 Recombination

By default, two established models for recombination are included in Driftfusion: band-to-band recombination and trap-mediated Shockley-Read-Hall recombination. The recombination expressions can be modified in the source terms of the Equation Editor (Section 5.5).

3.9.1 Band-to-band recombination

The rate of band-to-band recombination r_{btb} (also commonly termed direct, radiative or bimolecular recombination) is proportional to the product of the electron and hole densities at a given location such that:

$$r_{\text{btb}}(x, t) = B(n(x, t)p(x, t) - n_i^2), \quad (55)$$

where B is the band-to-band recombination rate coefficient. The n_i^2 term is equivalent to including an expression for thermal generation to ensure that $np \geq n_i^2$ at steady-state.

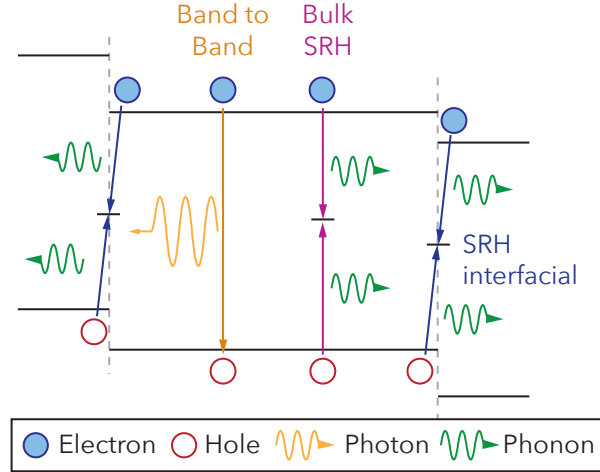


Fig. 5 Schematic of different recombination mechanisms in a HTL-i-ETL device. Trap-mediated Shockley Read Hall (SRH) recombination can be localised in the simulation whereas band-to-band recombination is implemented throughout all layers. Figure reproduced from [10].

3.9.2 Shockley-Read-Hall (SRH) recombination

Recombination via trap states is modelled using a simplified Shockley-Read-Hall (SRH) recombination[34] expression r_{SRH} for which the capture cross section, mean thermal velocity of carriers, and trap density are collected into SRH time constants, $\tau_{n,\text{SRH}}$ and $\tau_{p,\text{SRH}}$ for electrons and holes respectively:

$$r_{\text{SRH}}(x, t) = \frac{n(x, t)p(x, t) - n_i^2(x)}{\tau_{n,\text{SRH}}(x)(p(x, t) + p_t(x)) + \tau_{p,\text{SRH}}(x)(n(x, t) + n_t(x))}, \quad (56)$$

where n_t and p_t are parameters that define the dependence of the recombination rate to the trap level and are given by the densities of electrons and holes when their respective QFLs are at the position of the trap energy, E_t :

$$n_t = n_i \exp\left(\frac{E_i - E_t}{k_B T}\right) \quad (57)$$

$$p_t = n_i \exp\left(\frac{E_t - E_i}{k_B T}\right) \quad (58)$$

It should be noted that Equation 56 is valid only when trapped carriers are in thermal equilibrium with those in the bands. It follows that the rate of trapping and de-trapping of carriers is assumed to be fast (ps - ns) compared to the timescale typically of interest for optoelectronic measurement protocols (> ns), such that the approximation is reasonable. In the current version of Driftfusion we also assume

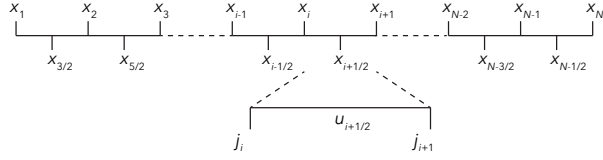


Fig. 6 The computational grid. Variables are solved for on the subintervals while flux densities are calculated on the integer intervals. Figure concept taken from Ref [12].

that the quantity of trapped carriers is negligible compared to that of the free carriers such that trapped carriers can be neglected in Poisson's equation. To more completely simulate the dynamics of capture and emission of carriers, and the associated contribution to the chemical capacitance of devices, one or more additional variables could be included.

The volumetric recombination rate can be obtained from a Driftfusion solution structure using the command:

```
r = dfana.calcrc(sol);
```

`r` is a structure containing three matrices `r.btb`, `r.srh`, and `r.tot` in which the band-to-band, SRH and the total recombination rates are stored as two dimensional matrices with dimensions of [time, space].

The recombination models used in the simulation can be edited using the carrier source terms `S_electron`, `S_hole`, `S_cation`, and `S_anion` in the equation editor in `dfpde` subfunction of the core `df` code. See Subsection 5.5 for further details.

3.10 Spatial mesh

Owing to the use of a finite element discretisation scheme the details of the spatial mesh in Driftfusion are of critical importance to ensure fast and reliable convergence. Multiple spatial mesh configurations, including non-linear piece-wise meshes are available and are described in the comments of `meshgen.x.m`.

The computational grid is divided into N intervals with $N - 1$ subintervals, where the position of the subintervals is defined by $x_{i+1/2} = (x_{i+1} + x_i)/2$ for $i = 1, 2, 3, \dots, N - 1$. `pdepe` solves for the variable values $u_{i+1/2}$ on the subintervals ($x_{i+1/2}$) and their associated flux densities j_i on the integer intervals (x_i) as illustrated in Figure 6.

The solution is interpolated for the integer grid points when generating the output solution matrix `sol.u` (see Section 5.6).

3.11 Time mesh

`pdepe` uses an adaptive time step for forward time integration and solution output is interpolated for the user-defined time mesh. While convergence of the solver is independent of the user-defined time mesh interval spacing, it is strongly dependent on the maximum time and the maximum time step. These can be adjusted by changing the `tmax` and `MaxStepFactor` properties of the parameters object (see Section 5.2).

4 Validation against existing models

To verify the numerical accuracy of the simulation, results from Driftfusion were compared against those from two analytical and two numerical models. In Section 4.1 current-voltage characteristics obtained using analytical and numerical solutions for a p-n junction solar cell are compared. In Section 4.2 the simulation's time integration is verified by calculating the transient photovoltage response of a single, field-free layer and comparing it to the solution obtained using a zero-dimensional kinetic model. Numerical solutions obtained using Driftfusion were also compared with those of an established commercially available package, the Advanced Semiconductor Analysis (ASA) simulation tool.[47] In section 4.3, the results for a three-layer, dual heterojunction device obtained from Driftfusion are compared with those obtained from ASA in order to verify that the different treatments of the interfaces produce equivalent results. Finally, in 4.4, J - V characteristics calculated using Driftfusion are compared with those of IonMonger, a recently published free-to-use three-layer semiconductor device simulator that includes the effects of mobile ionic carriers in the absorber layer.[14]

The location of the scripts and the parameter sets used to obtain the results in this section can be found in the Supplemental Information, Section 3.

4.1 The depletion approximation for a p-n junction

The p-n junction depletion approximation The Depletion Approximation (DA) allows the continuity equations and Poisson's Equation (Equations 26, 27 and 16) to be solved analytically for a p-n homojunction.[33] The depletion region at the junction of the device is assumed to have zero free carriers such that the space charge density ρ can be described using a step function with magnitude equal to

the background doping density (see Figure 7a, top panel). Transport and recombination of free carriers in the depletion region is also ignored. Poisson's equation can then be solved by applying fixed carrier density ($p(x = -\infty) = p_0$ and $n(x = \infty) = n_0$) and zero-field boundary conditions to obtain the depletion widths for n- and p-type regions, w_n and w_p respectively:[36]

$$w_n = \frac{N_A}{N_A + N_D} \sqrt{\frac{2\epsilon_r\epsilon_0 V_{bi}}{q \left(\frac{1}{N_A} + \frac{1}{N_D} \right)}} \quad (59)$$

$$w_p = \frac{N_D}{N_A + N_D} \sqrt{\frac{2\epsilon_r\epsilon_0 V_{bi}}{q \left(\frac{1}{N_A} + \frac{1}{N_D} \right)}} \quad (60)$$

Solving the DA for the current flowing across the junction under the assumption that the diffusion length of both carriers is significantly greater than the device thickness ($L_{n,p} \gg d$) yields the *Shockley diode equation*:

$$J = J_0 \left(\exp \left(\frac{qV_{app}}{k_B T} \right) - 1 \right) - J_{SC}, \quad (61)$$

where J_{SC} and J_0 are the short circuit and dark saturation current densities respectively. Here we use the convention that a positive applied (forward) bias generates a positive current flowing across the junction.

To make the comparison between numerical and analytical current-voltage (J - V) characteristics, values for J_0 and J_{SC} need to be related to input parameters for the simulation. J_0 embodies the recombination characteristics of the device. For the contribution to recombination in the quasi-neutral region, J_0 can be related to the electron and hole diffusion lengths L_n and L_p , minority carrier lifetimes τ_n and τ_p , and diffusion coefficients D_n and D_p , according to:[36]

$$J_0 = \frac{qD_p p_{0,n-type}}{L_p} + \frac{qD_n n_{0,p-type}}{L_n} \quad (62)$$

where $L_p = \sqrt{\tau_p D_p}$ and $L_n = \sqrt{\tau_n D_n}$.

The material band gap and AM1.5 solar spectrum were used to calculate the theoretical maximum current density $J_{SC,max}$ and corresponding uniform generation rate throughout the depletion region g_0 . Figure S.2 of the Supplemental Information shows the AM1.5 Global Tilt solar spectrum obtained from Ref.[6] used for the calculation.

The limiting short circuit photocurrent for a perfectly absorbing semiconductor of band gap E_g is given by:[26]

$$J_{SC}(E_g) = q \int_0^\infty \eta(E_\gamma) \phi_0(E_\gamma) dE_\gamma, \quad (63)$$

where η is the external quantum efficiency. If $\eta = 1$ for photon energies $E_\gamma \geq E_g$, and $\eta = 0$ for $E_\gamma < E_g$, the maximum theoretically achievable short circuit current for a single junction $J_{SC,max}$ is given by the integral of ϕ_0 from the bandgap energy to infinity. Figure S.2 of the Supplemental Information shows the maximum achievable current density $J_{SC,max}$ over a range of band gap energies. For the comparison we use the bandgap of silicon $E_g = 1.12$ eV resulting in $J_{SC,max} = 42.7$ mA cm⁻².

Simulation methods A p-n junction was devised in Driftfusion with very thick n- and p-type layers (≈ 100 μ m, $p_0 \approx N_A = 9.47 \times 10^{15}$ cm⁻³, $n_0 \approx N_D = 2.01 \times 10^{15}$ cm⁻³) to approximate the assumptions and boundary conditions used in the DA. Furthermore, ionic carriers and trapped electronic charges are not included in the simulations in this section. The surface recombination velocity was set to zero for minority carriers at both boundaries. A special recombination scheme was implemented using the following simplified first order expressions:

$$r = \frac{n - n_0}{\tau_n} \quad \text{for } x < d/2 - w_p \quad (64)$$

$$r = \frac{p - p_0}{\tau_p} \quad \text{for } x > d/2 + w_n, \quad (65)$$

where τ_n and τ_p are the electron and hole lifetimes respectively. For simplicity, τ_n and τ_p were set equal to one another and, for consistency with the DA, recombination was switched off in the depletion region.

To convert the value obtained for $J_{SC,max}$ into a uniform carrier generation rate, the short circuit flux density ($j_{SC,max} = J_{SC,max}/q$) was divided by the depletion region thickness d_{DR} , yielding $g_0 = j_{SC,max}/d_{DR}$. The complete parameter sets for the simulations in this section are given in Tables S.5 and S.6.

Results Both the analytical and numerical solutions for the space charge density, electric field, and electric potential are shown in Figure 7: The space charge widths, field strength and potential profiles all show good agreement.

Figure 8 shows the light and dark current-voltage curves for the analytical solution obtained using equation 61, as compared to the numerical solutions from Driftfusion for three values of $\tau_{n,p}$. For $\tau_{n,p} = 10^{-6}$ and $\tau_{n,p} = 10^{-7}$ the agreement is very good, even at current densities as low as 10^{-14} A cm⁻². The solutions begin to diverge at $\tau_{n,p} = 10^{-8}$, for which $L_{n,p} = 2.3 \times 10^{-3}$ cm such that $L_{n,p} \ll d$ and the underlying assumptions of the DA are no longer valid. The deviation from the ideal model in Driftfusion at higher current densities (inset) is expected due to the absence of series resistance in the DA.

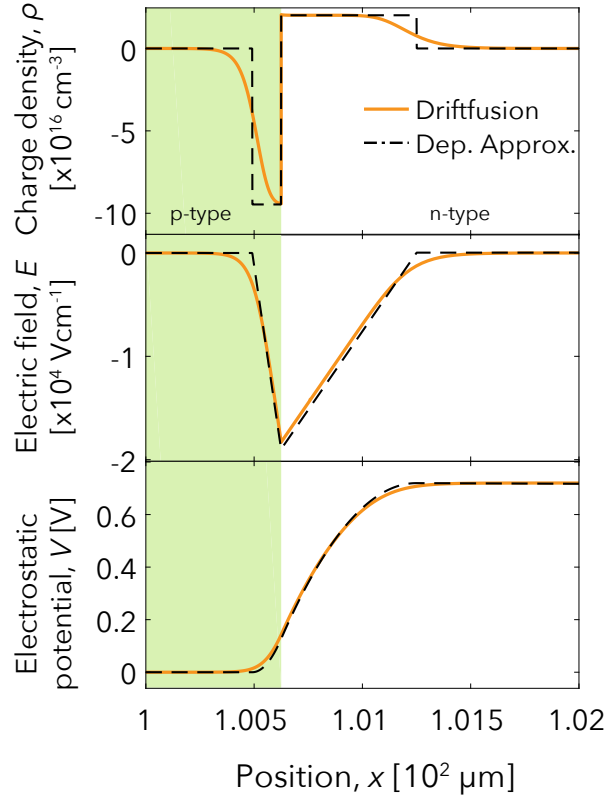


Fig. 7 Analytical and numerical solutions of a p-n junction. Solutions obtained from Driftdiffusion (solid orange curve) and the depletion approximation (Dep. Approx., dashed black curve) for a p-n junction with $E_g = 1.12$ eV and $N_A = 9.47 \times 10^{15} \text{ cm}^{-3}$, $N_D = 2.01 \times 10^{15} \text{ cm}^{-3}$. Green and white regions indicate the n-type and p-type layers respectively. The complete parameter sets for the simulations are given in Tables S.5 and S.6.

4.2 Transient photovoltage response of a single layer field-free device

Analytical methods To verify the time-dependence of the solution from Driftdiffusion, the transient photovoltage (TPV) response for a field-free slab of intrinsic semiconductor was calculated numerically and compared to results from a zero-dimensional (0-D) kinetic model. During a TPV experiment the device is illuminated at open circuit with a constant bias light and pulsed with an optical excitation source such as to produce a small additional photovoltage ΔV . As detailed in Supplemental Information Section 3.2.1, it can be shown using a kinetic model that ΔV is given by:

$$\Delta V_{OC} = \frac{2k_B T}{q n_{OC}} \frac{\Delta g}{k_{TPV}} (1 - \exp(-k_{TPV}(t + t_{pulse}))) \quad \text{for } -t_{pulse} < t \leq 0, \quad (66)$$

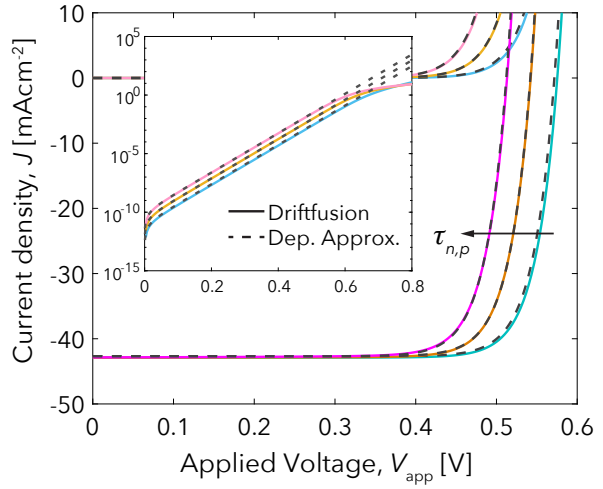


Fig. 8 Comparison of current-voltage characteristics obtained using Driftdiffusion and the Depletion Approximation for a p-n junction. Current-voltage characteristics for numerical and analytical solutions for a p-n junction with $\tau_n = \tau_p = 10^{-6}$, 10^{-7} , and 10^{-8} s. Results from Driftdiffusion and the Depletion Approximation (Dep. Approx.) are denoted by solid and dashed lines respectively. The complete parameter sets for the simulations are given in Tables S.5 and S.6. The dark currents are shown on a logarithmic scale in the inset.

$$\Delta V_{OC} = \frac{2k_B T}{q n_{OC}} \exp(-k_{TPV} t) \quad \text{for } t > 0, \quad (67)$$

where t_{pulse} is the length of the laser pulse, Δg is the additional volumetric generation rate due to the excitation pulse, n_{OC} is the steady-state open circuit carrier density, and k_{TPV} is the decay rate constant of the TPV signal.

Simulation methods A 100 nm field-free single layer of semiconductor with $E_g = 1.6$ eV was simulated in Driftdiffusion with the zero flux density boundary conditions for electronic carriers representing perfect blocking contacts. The ionic carrier density was set to zero throughout. The constant volumetric generation rate was set to $g_0 = 1.89 \times 10^{21} \text{ cm}^{-3} \text{ s}^{-1} = 1$ sun equivalent based on the integrated photon flux density for the AM1.5G solar spectrum and a step function absorption. In this special case the splitting of the Fermi levels in the simulation is solely attributable to changes in chemical potential, such that no series resistance term is needed for the potential boundary conditions. It should be noted that for instances where an electric field is present in the device these boundary conditions will not represent an open circuit condition; a high value for R_s or a mirrored cell approach (see Ref. [8] for details) should be used instead. The second order band-to-band recombination coefficient was set to $B = 10^{-10} \text{ cm}^3 \text{ s}^{-1}$ and SRH recombination was switched

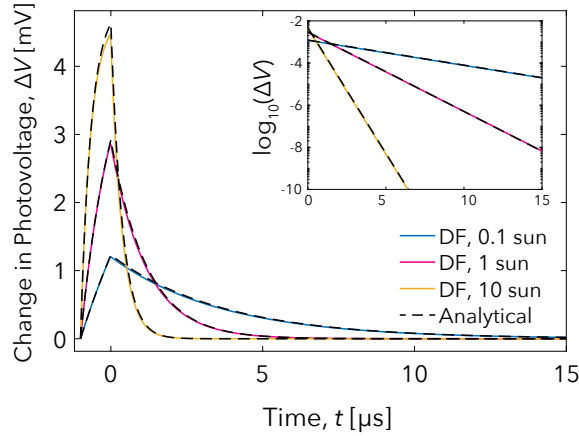


Fig. 9 Zero-dimensional theoretical prediction versus 1-D numerical drift-diffusion simulations for the transient photovoltage response of a single layer of semiconductor. Transient photovoltage as a function of time calculated using Driftfusion (DF, solid curves) and a zero-dimensional kinetic model (Analytical, black dashed curves) at bias light intensities of 0.1, 1, and 10 sun equivalent. The pulse length was $1 \mu\text{s}$ and the pulse intensity was set to be 20% of the bias intensity in each instance. The inset shows the results on a \log_{10} scale. The complete parameter sets for the simulations are given in Tables S.7 and S.8.

off. Since the underlying kinetic theory demands that the TPV perturbation must be small such that the additional carrier density $\Delta n \ll n_{\text{OC}}$, we used $t_{\text{pulse}} = 1 \mu\text{s}$ and set the pulse intensity equivalent to be 20% of the bias light intensity. The complete parameter sets for the simulations are given in Tables S.7 and S.8.

Results The results of the comparison between theory and simulation for light intensities of 0.1, 1, and 10 sun equivalent are given in Figure 9. The steady-state charge carrier densities and open circuit voltage obtained using Driftfusion agreed to within 10 decimal places with the analytical values calculated using Equations S.4 and S.3 ($n = 4.35 \times 10^{15} \text{ cm}^{-3}$, $V_{\text{OC}} = 1.08 \text{ V}$ (3 s.f.) at 1 sun equivalent). The transient photovoltage perturbations also behaved as predicted, with the rate constants extracted from fitting the TPV decays correct to within 3 significant figures of the values calculated using the analytical expression in Equation 67.

4.3 Numerical solution for three-layer devices without mobile ions

Simulation methods To verify that the graded treatment of the interfaces in Driftfusion produces similar results to models that use abrupt interfaces, a HTL/absorber/ETL device was simulated using both Driftfusion and the Advanced Semiconductor Analysis (ASA) simulation tool.[47] To maintain consistent layer dimensions the linear grid

spacing for the ASA simulations and the interface thickness in Driftfusion were set to be 1 nm.

The base material parameters for the active layer were based loosely on those for a perovskite material excluding mobile ionic charge. The parameters for the contact layers were not chosen to simulate real materials but rather to ensure a large built-in potential and to vary as many properties as possible including the layer thickness, dielectric constants, recombination coefficients, mobilities etc. For optical generation the Beer-Lambert option (without back contact reflection) was chosen and the same optical constant and incident photon flux density spectrum data were used in both simulators. Four different parameter sets (PS) were compared, the key differences for which are summarised in the first four columns of Table 1.

The complete parameter sets for the simulated devices are given in Tables S.9 - S.12.

Results: Beer-Lambert optical model The results for the integrated generation rate profiles are shown in Figure 10. Despite the wavelength-dependent generation rates appearing to be very closely matched between the two simulators (Figure S.4), the integration across photon energies resulted in marginally different generation profiles in the two simulations corresponding to a total difference in generation current of 1.24 mA cm^{-2} . As a means to ensure that the input generation profiles were identical, the generation profile from ASA was inserted into the Driftfusion parameters objects using the method described in Section 5.2.6.

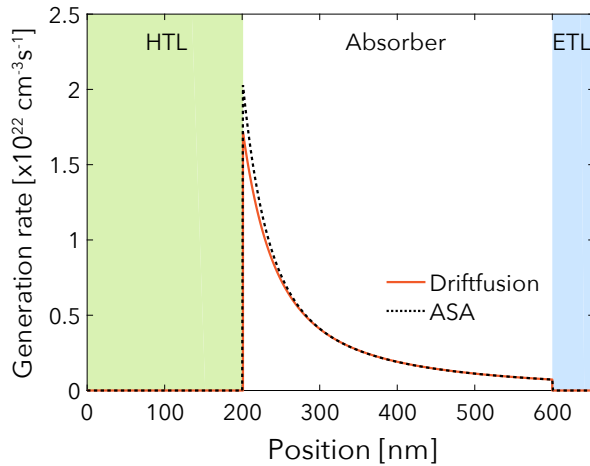


Fig. 10 Integrated generation profile obtained using Driftfusion and ASA Beer Lambert models.

Results: Current-voltage characteristics To compare the current outputs from the different simulation tools current-voltage scans were performed from $V_{\text{app}} = 0$ to 1.3 V. Since

Table 1 Summary of the key simulation parameters for comparison of Driftdiffusion with ASA. CB and VB indicate the conduction and valence bands respectively.

Parameter set	Description	Built-in voltage (V)	Active layer thickness (nm)	CB and VB effective density of states (cm^{-3})		
				HTL	Absorber	ETL
1a	3-layer device based on MAPI active layer	1.05	400	10^{19}	10^{18}	10^{19}
1b	As 1a with thinner active layer	1.05	200	10^{19}	10^{18}	10^{19}
2a	Randomised layer properties	0.6	200	10^{19}	10^{18}	10^{20}
2b	As 2a with uniform eDOS all layers	0.6	200	10^{18}	10^{18}	10^{18}

ASA solves for the steady-state current, the J - V scan rate was set to be low ($k_{\text{scan}} = 10^{-10} \text{ V s}^{-1}$) in Driftdiffusion to minimise contributions from the displacement current.

Figure 11a shows a comparison of the J - V characteristics obtained from the two simulation tools for Parameter Sets (PS) 1a and 2a. While the different parameter sets result in distinctly different characteristics for the two devices, the data show excellent agreement between the two simulators despite the significant difference in discretisation schemes and interface treatment.

Closer examination of the results from the two simulators (Figure 11b) reveals that, while the absolute difference (calculated as $100 \times |(J_{\text{ASA}} - J_{\text{DF}})/J_{\text{ASA}}|$) for PS 1a is on the order of 1 % beyond current densities above approximately $J = 10^{-12} \text{ A cm}^{-2}$, the difference for PS 2a is much greater at ≈ 10 %. This difference is decreased marginally by increasing the point spacing density in ASA from 1 to 4 points per nm (Figure S.7). In part, the difference between the two simulation tools can be attributed to a change of over 7 orders of magnitude in the electron density at the absorber-ETL interface (Figure S.8) due to both a transition in the conduction band eDOS from $N_{\text{CB}} = 10^{18}$ to 10^{20} cm^{-3} and a change in the conduction band energy of 0.3 eV. Under these circumstances the difference in discretisation schemes between the two tools becomes apparent. The deviation is reduced significantly (by approximately two-thirds) by using a uniform eDOS of $N_{\text{CB}} = 10^{18} \text{ cm}^{-3}$ across all layers as the results for PS 2b show. We note that despite the difference in results for PS 2a, the key metrics of the J - V curve such as the V_{OC} , ideality factor and fill-factor are preserved.

Figure 12 shows a comparison of the electrostatic potential and hole density profiles calculated using Driftdiffusion and ASA for PS 1a under illumination at increasing applied bias. The electron density is given in the Supplemental Information, Figure S.9. Again the agreement between the solutions is excellent taking into consideration the difference in treatment of the interfaces between the two simulators, namely that ASA uses abrupt interfaces between different material layers while Driftdiffusion uses interfaces with graded properties.

4.4 Numerical solution for a three-layer device with mobile ions

Methods Courtier et al. recently published IonMonger,[14] a three-layer drift-diffusion code for simulating perovskite solar cells which solves for coupled electron, hole and a single ionic carrier distributions. In contrast to Driftdiffusion, IonMonger uses abrupt interfaces and solves carriers and the electrostatic potential for the three device layers simultaneously. This approach establishes boundary conditions between the absorber and transport layers, and thus supports recombination terms between electrons and holes at remote nodes, i.e. at grid points either side of the interfaces. Here we compare results obtained from Driftdiffusion with those from IonMonger using a similar parameter set to the default set of IonMonger. Since the treatment of the interfaces is different between the two codes, mobile ionic charge is excluded from the interfaces in Driftdiffusion by setting the mobility for ionic carriers to zero in these regions, using the zeroing option in the device builder (see Section 5.2.4). This modification allows for a more direct comparison of the ionic carrier profiles in the perovskite region. We note that inclusion of the ionic charge in the interfaces makes little difference to the extracted photocurrent (Supplemental Information, Figure S.14). Owing to the differences in how the two codes treat the interfaces, interfacial recombination was also switched off in both simulators.

Results: Current-voltage characteristics Figure 13a shows the J - V scan results from Driftdiffusion and IonMonger using the test parameter set at scan rates of $k_{\text{scan}} = 0.1, 1$, and 10 V s^{-1} . Figure 13b - d shows the electrostatic potential profile, ionic carrier accumulation and hole profiles during the 1 V s^{-1} forward scan at increasing applied bias. The corresponding electron densities are given in the Supplemental Information Figure S.16. While the results of the two simulations are qualitatively similar, there are differences in the calculated ionic charge carrier densities that result in small differences to the electrostatic potential and current outputs. This variance likely arises from three key differences between the simulators; 1. The treatment of electronic currents across the interfaces; 2. Calculation of ionic carrier densities throughout all layers of the device in Driftdiffusion as opposed

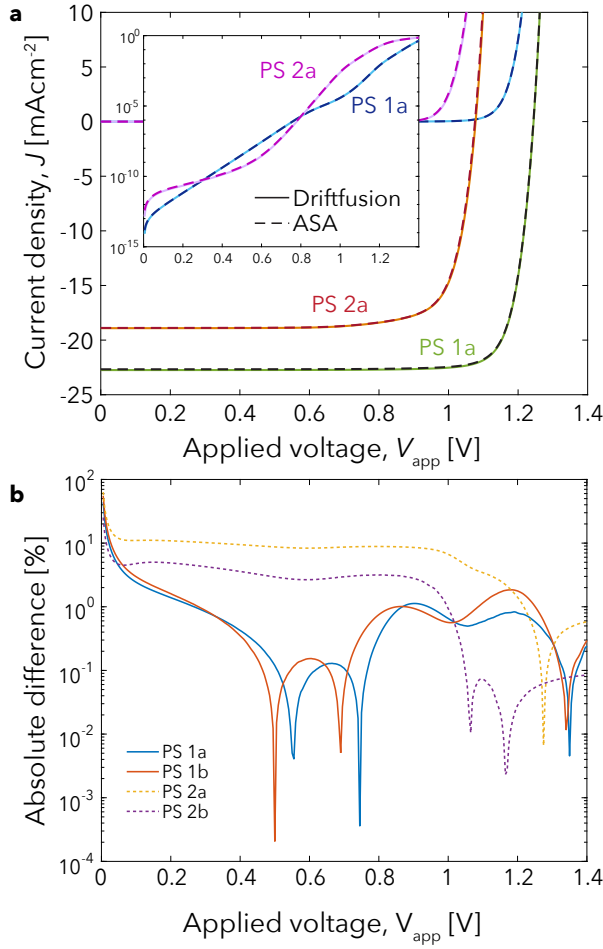


Fig. 11 Comparison of dark and light current-voltage characteristics calculated by Driftfusion and ASA **a** Current-voltage characteristics for Parameter Sets (PS) 1 and 2. Inset dark currents shown on log scale. Dashed and solid lines indicate the current calculated using Driftfusion and ASA respectively. **b** Percentage difference between dark current calculated using Driftfusion and ASA for the 4 different parameter sets investigated. The complete parameter sets for the simulations are given in Tables S.9 - S.12.

to IonMonger, which only calculates ionic carriers in the absorber layer. While this has the advantage that penetration of ionic carriers into other layers can be investigated in Driftfusion, it has the disadvantage that small additional integration errors are introduced into the ionic space charge density (Supplemental Information Figure S.15); 3. Minority carrier capacitances in the interfaces and transport layers present in Driftfusion, which are not accounted for in IonMonger.

While IonMonger might be expected to produce a solution more consistent with an abrupt interface analytical model, the inclusion of minority carrier densities in the transport regions and, arguably the interface treatment, is more physically meaningful in Driftfusion. Consistency with established analytical models that use abrupt interfaces

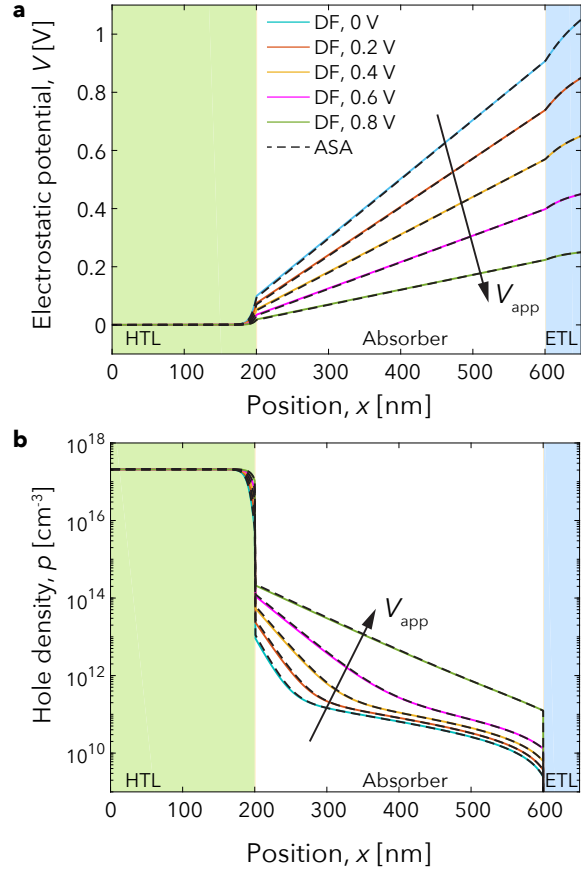


Fig. 12 Comparison of the electrostatic potential and hole density profiles during a J - V scan for a three-layer device calculated by Driftfusion and ASA. Results from Driftfusion indicated by solid lines whereas results from ASA are indicated by dashed lines. Corresponding electron densities are given in Supplemental Information Figure S.9.

is somewhat sacrificed in Driftfusion in favour of greater flexibility, which enables the physical models to be easily edited, more than three layers to be simulated and a range of interface-specific properties and grading functions to be specified. Taking into consideration these modifications, the results comparison with IonMonger remains very good.

In summary, we have verified Driftfusion against two analytical and two existing numerical models and found that in all cases the calculated results are in good agreement. In the following and final section the system architecture and functions are introduced as well as a guide on how to get started with using Driftfusion.

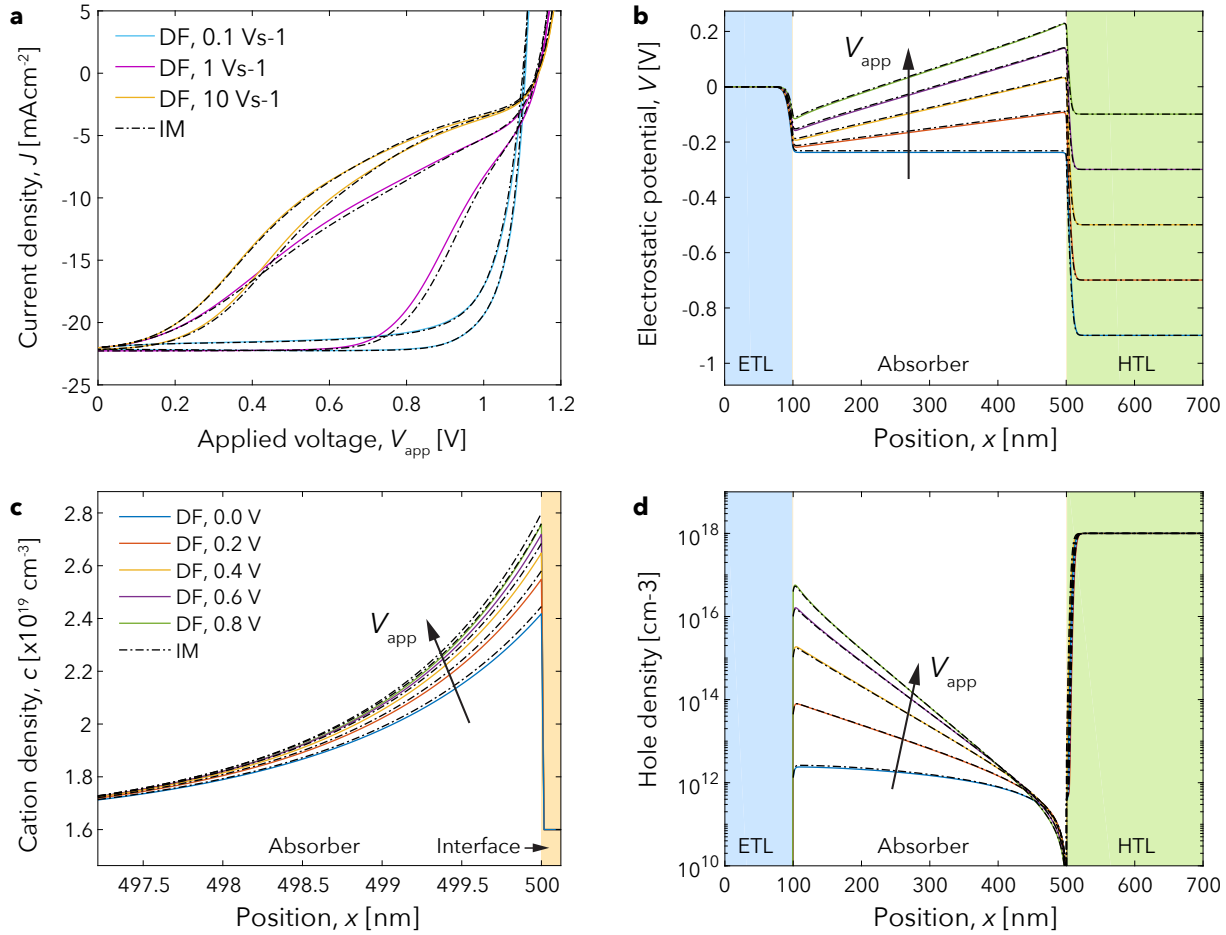


Fig. 13 Comparison of results calculated using Driftfusion and IonMonger for a three-layer solar cell including mobile ionic carriers in the absorber layer. (a) Current-voltage scans at $k_{scan} = 0.1, 1$, and 10 V s^{-1} . (b) The electrostatic potential (c) Cation density, and (d) Hole density profiles at increasing voltage during the 1 V s^{-1} forward scan. Results from Driftfusion (DF) are indicated by solid coloured lines, whereas those from IonMonger (IM) are indicated by dashed black lines. The complete parameter sets for the simulations are given in Tables S.13 and S.14.

5 System architecture and how to use Driftfusion

Driftfusion is designed such that the user performs an linear sequence of simple procedures to obtain a solution. The key steps are summarised in Figure 14; Following initialisation of the system, the user defines a device by creating a parameters object containing all the individual layer and device-wide properties; The equilibrium solutions (`soleq.e1` and `soleq.ion`) for the device are then obtained before applying a voltage and light protocol, which may involve intermediate solutions; Once a final solution (`sol`) has been obtained, analysis and plotting functions can be called to calculate outputs and visualise the solutions. Below, the principal functions are discussed in further detail.

5.1 Initialising the system: `initialise_df`

At the start of each MATLAB session, `initialise_df` needs to be called from within the Driftfusion parent folder (*not one of its subfolders*) to add the program folders to the file path and set plotting defaults. This action must be performed before any saved data objects are loaded into the MATLAB workspace to ensure that objects are associated with their corresponding class definitions.

5.2 Defining device properties and creating a parameters object: `pc(file_path)`

The parameters class, `pc` contains the default device properties and functions required to build a parameters object, which we shall denote herein as `par`. The parameters object defines both layer-specific and device-wide properties.

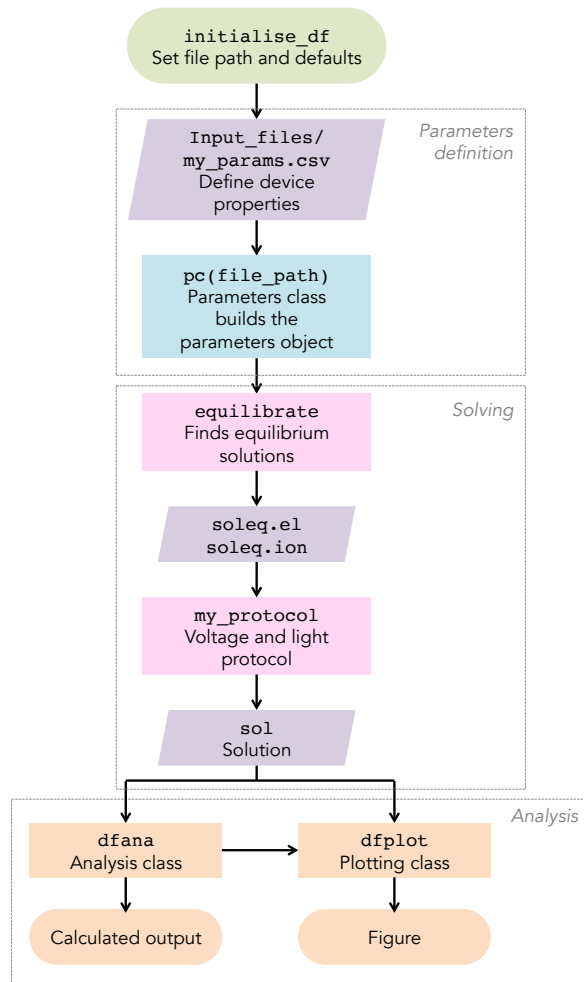


Fig. 14 Flow diagram showing the key steps to obtain a solution. A key for the classification of the box shapes is given in Figure 15.

Layer-specific properties must be a cell or numerical array containing the same number of elements as there are layers, *including* interface (junction) layers. For example, a three-layer device with two heterojunctions requires layer-specific property arrays to have five elements. Examples can be found in the `/Input_files` folder (see Section 5.2.1).

Figure 15 shows the processes through which the main components of the parameters object are built; The user is required to define a set of material properties for each layer. The comments in `pc` describe each of the parameters in detail and give their units (also see Supplemental Information, Table S.3 for quick reference); Several subfunctions (methods) of `pc` then calculate dependent properties, such as the equilibrium carrier densities and the bandgap energies for example, from the choice of probability distribution function (`prob_distro_function`) and other user-defined properties. The treatment of properties in the device inter-

faces is dealt with, and can be changed, using the device builder `build_device` (see below).

5.2.1 Importing properties

Typically, the most important user-definable properties are stored in a `.csv` file, which is easily editable with a spreadsheet editor such as LibreOffice or Microsoft Excel. The file path to the `.csv` file can be used as an input argument for `pc` e.g.

```
par = pc('Input_files/spiro_mapi_tio2.csv');
```

This allows the user to easily create and store new parameter objects without editing `pc`. Default values for properties set in the parameters class `pc` will be overwritten by the values in the `.csv` file during creation of the parameters object `par`. New properties defined in `pc` can easily be added to the `.csv` file provided that they are also included in the `import_properties` function which tests to see which properties are present in the text file and reads them into the parameters object where present. To avoid potential incompatibility, new user-defined material properties, which have distinct values for each layer, should be included in the `.csv` file and added to the list of importable properties in `import_properties`. An example of how to do this is given in the Supplemental Information, Section 5.

5.2.2 Layer types

Layer types, set using the `layer_type` property, flag how each layer should be treated. Driftfusion currently uses three layer types:

1. 'layer' is a slab of semiconductor for which all properties are spatial constant.
2. 'active' is the same as layer but flags the active layer of the device. The number of the first layer designated 'active' is stored in the `active_layer` property and is used for calculating further properties such as the active layer thickness, `d_active`. Flagging the active layer proves particularly useful when automating parameter explorations as the active layer can easily be indexed.
3. 'junction' indicates an interface between two materials. The properties of a graded junction are varied according to the specific choice of grading method as defined in `build_device` (see below).

5.2.3 Spatial mesh generator

`meshgen_x` creates integer and subinterval spatial meshes, `x` and `x_ihalf` respectively, based on the layer widths and number of points defined in the device properties, and the mesh type. The property `xmesh_coeff` controls the spread

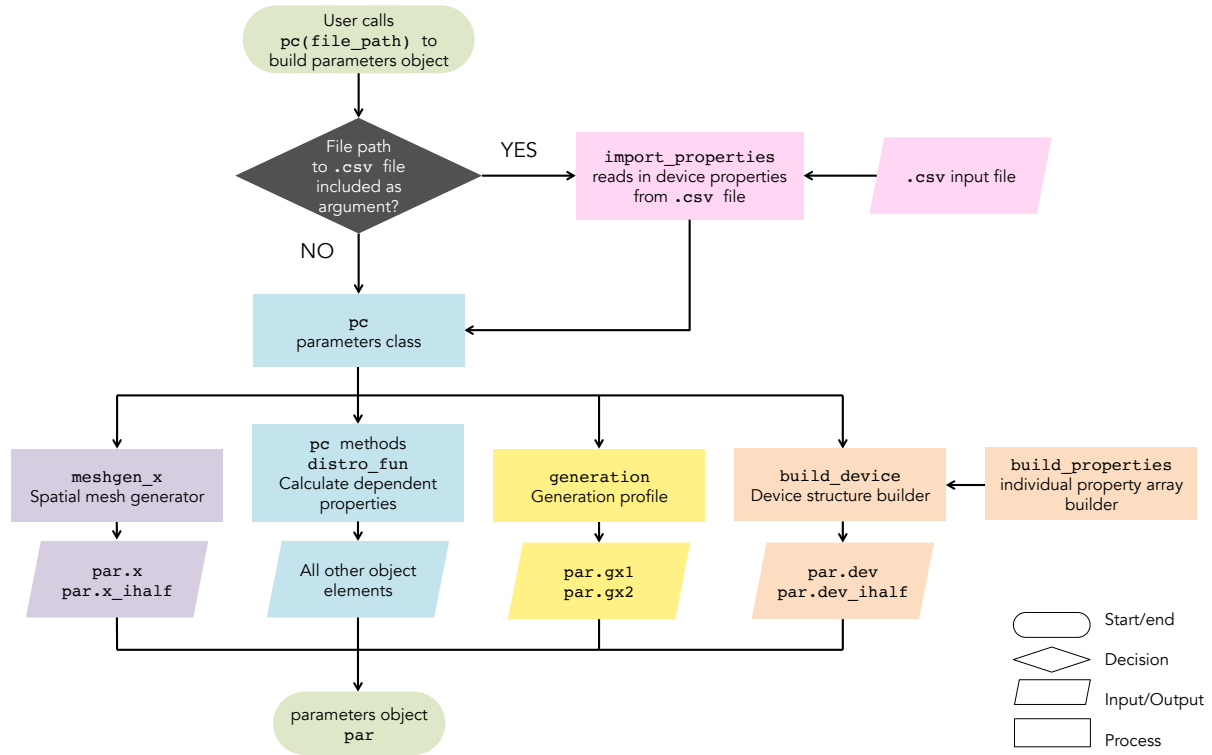


Fig. 15 Flow diagram showing the key processes involved in building a parameters object.

of points for meshes where non-linear spacing is used. Further details can be found in the code comments for `meshgen_x`.

5.2.4 The device structures

The device structures `dev` and `dev_ihalf` are required by the master function `df` to reference material properties at each spatial grid point when solving the equations. `build_device` and `build_property` are called during creation of the parameters object to build two structures: `dev`, defined on the integer grid intervals (x_i), is used to define the initial conditions only, while `dev_ihalf`, defined on the subintervals ($x_{i+\frac{1}{2}}$), is used by the `pdepe` solver function. `build_property` enables the user to specify different types of interface grading for each property listed in `build_device`. At present there are four grading option types:

1. 'zeroed': The value of the property is set to zero throughout the interfacial region.
2. 'constant': The value of the property is set to be constant throughout the interfacial region. Note that the user must define this value in the `.csv` file. See the default settings for the electron and hole SRH lifetimes `taun` ($\tau_{n,SRH}$) and `taup` ($\tau_{p,SRH}$) properties in any of

the default three-layer device parameter sets in the `/Input_files` folder for examples.

3. 'lin_graded': The property is linearly graded using the property values of the adjoining layers.
4. 'log_graded': The property is exponentially graded using the property values of the adjoining layers.

The `build_device` function contains the default grading type for each property e.g. the default grading type for the electron affinity, Φ_{EA} is 'lin_graded', while that for the intrinsic carrier density, n_i is 'log_graded'.

5.2.5 The electronic carrier probability distribution function

`distro_fun` defines the electronic carrier probability distribution function for the device and calculates carrier densities and diffusion coefficients. At present only Boltzmann statistics are available for use in Driftdiffusion with future plans for the inclusion of alternative statistical distributions.

5.2.6 The electronic carrier generation profile function

`generation` calculates the two generation profiles `gx1` and `gx2`, which can be used for a constant bias light and a pulse source for example, at each spatial location in the device

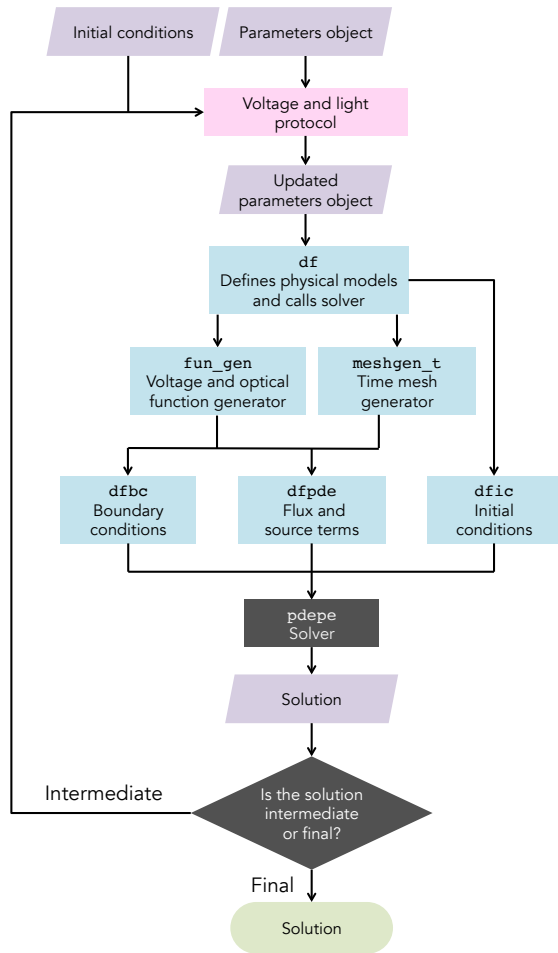


Fig. 16 Flow diagram illustrating execution of a Driftfusion protocol.

for the chosen optical model and light sources (see Section 3.8 and the flow diagram in the Supplemental Information Figure S.17). The light sources can be set using the `light_source1` and `light_source2` properties.

A arbitrary generation profile calculated using an external program (such as Solcore[1] or the McGeeHee Group's Transfer Matrix code[5]) can be inserted into the parameters object `par` by overwriting the generation profile properties `gx1` or `gx2` following creation of the object. The profile must be interpolated (using the `interp1` MATLAB function for example) for the subinterval $(x_{i+1/2})$ grid points defined by `x_ihalf` (see Section 3.10).

The time-dependence of the light sources is controlled using the `g1_fun_type` and `g2_fun_type` properties, which define the function type e.g. sine wave, and the `g1_fun_arg` and `g2_fun_arg` properties, which are coefficients arrays for the function generator (see Section 5.5.5) e.g. the frequency, amplitude, etc.

5.3 Protocols: equilibrate

Once a device has been created and stored in the MATLAB workspace as a parameters object the next step is to find the equilibrium solution for the device. The function `equilibrate` starts with the initial conditions described in Section 3.7 and runs through a number of steps to find the equilibrium solutions, with and without mobile ionic carriers, for the device described by `par`. The output structure `soleq` contains two solutions (see Section 5.6);

1. `soleq.el`: only the electronic charge carriers have been made mobile and are at equilibrium.
2. `soleq.ion`: electronic and ionic carriers have been made mobile and are at equilibrium.

Storing both solutions in this way allows devices with and without mobile ionic charge to be compared easily.

5.4 Protocols: General

A Driftfusion protocol is defined as a function that contains a series of instructions that takes an input solution (initial conditions) and produces an output solution. For many of the existing protocols, listed in Table 2, with the exception of `equilibrate`, the input is one of the equilibrium solutions, `soleq.el` or `soleq.ion`. Figure 16 is a flow diagram illustrating the key functions called during execution of a protocol.

Protocols typically start by creating a temporary parameters object that is a duplicate of the input solution parameters object. This temporary object can then be used to write new voltage and light parameters that will be used by the function generator to define the generation rate at each point in space and time and the potential at the boundary at each point in time. Additional parameters, for example those defining the output time mesh or carrier transport are also frequently adjusted. The approach is to split a complex experimental protocol into a series of intermediate steps that facilitate convergence of the solver. For example, where ionic mobilities are separated by many orders of magnitude from electronic mobilities, a steady-state solution is easiest found by accelerating the ions to similar values to the electronic carriers using the `K_anion` and `K_cation` properties. The simulation can then be run with an appropriate time step and checked to ensure that a steady-state has been reached. The possibilities are too numerous to list here and users are encouraged to investigate the existing protocols listed in Table 2 in preparation of writing their own.

5.5 The master function `df`

`df` is the core function of Driftfusion. `df` takes the device parameters, and voltage and light conditions, calls the solver

Table 2 List of protocols available in Driftdiffusion at the time of publication.

Command	Description
<code>changeLight</code>	Switches light intensity using incremental intensity steps.
<code>doCV</code>	Cyclic Voltammogram (CV) simulation using triangle wave function generator .
<code>doIMPS</code>	Intensity Modulated Photocurrent Spectroscopy (IMPS) simulation at a specified frequency and light intensities.
<code>doIMVS</code>	Switches to open circuit (OC), runs to steady-state OC, then performs Intensity Modulated Photovoltage Spectroscopy (IMVS) measurement simulation at a specified frequency and light intensities.
<code>doJV</code>	Forward and reverse current-voltage (JV) scan with options for dark and constant illumination conditions.
<code>doLightPulse</code>	Uses light source 2 with square wave generator superimposed on light source 1 (determined by the initial conditions) to optically pulse the device.
<code>doSDP</code>	Step, Dwell, Probe (SDP) measurement protocol: Jump to an applied potential, remain at the applied potential for a specified dwell time and then perform optically pulsed current transient. See Ref. [3] for further details of the experimental protocol.
<code>doSPV</code>	Surface PhotoVoltage (SPV) simulation: Switches light on with high series resistance.
<code>doTPV</code>	Transient PhotoVoltage (TPV) simulation: Switches to open circuit with bias light and optically pulses the device.
<code>equilibrate</code>	Start from base initial conditions and find equilibrium solutions without mobile ionic charge (<code>soleq.e1</code>) and with mobile ionic charge (<code>soleq.ion</code>).
<code>findVoc</code>	Obtains steady-state open circuit condition using Newton-Raphson minimisation.
<code>findVocDirect</code>	Obtains an approximate steady-state open circuit condition using 1 M Ω series resistance.
<code>genIntStructs</code>	Generates solutions at various light intensities.
<code>genIntStructsRealVoc</code>	Generates open circuit solutions at various light intensities.
<code>genVappStructs</code>	Generates solutions at various applied voltages.
<code>jumpToV</code>	Jumps to a new applied voltage and stabilises the cell at the new voltage for a user-defined time period.
<code>lightonRs</code>	Switches on the light for a specified period of time with a user-defined series resistance.
<code>stabilize</code>	Runs a set of initial conditions to a steady-state.
<code>sweepLight</code>	Linear sweep of the light intensity over a user-defined time period.
<code>transient_nid</code>	Simulates a transient ideality factor (n_{id}) measurement protocol.
<code>VappFunction</code>	Applies a user-defined voltage function to a set of initial conditions.

and outputs the solution (Figure 16). The underlying equations in Driftdiffusion can be customised for specific models and applications using the Equation Editor in the `dfpde` subfunction. `df` contains three important subfunctions: `dfpde`, `dfic`, and `dfbc`:

5.5.1 Driftdiffusion Partial Differential Equation function `dfpde` and the Equation Editor

`dfpde` defines the equations to be solved by MATLAB's Partial Differential Equation: Parabolic and Elliptic solver toolbox (`pdepe`).[32] For one-dimensional Cartesian coordinates, `pdepe` solves equations of the form:

$$C\left(x, t, u, \frac{\partial u}{\partial x}\right) \frac{\partial u}{\partial t} = \frac{\partial u}{\partial x} \left(F\left(x, t, u, \frac{\partial u}{\partial x}\right) \right) + S\left(x, t, u, \frac{\partial u}{\partial x}\right) \quad (68)$$

Here, u is a vector containing the variables n , p , c , a , and V at a position in space x and time t . C is a vector defining the prefactor for the time derivative, F is a vector determining the flux density terms (note: F does *not* denote the electric field in this section), and S is a vector containing the source/sink terms for the components of u . By default $C = 1$ for charge carriers but could, for example, be used to change

the active volume fraction of a layer in a mesoporous structure. The equations can be easily reviewed and edited in the `dfpde` Equation Editor as shown in Listing 1. Here, device properties that have a spatial dependence are indexed with the variable i to obtain the corresponding value at the location given by `x_ihalf(i)`. A step-by-step example of how to change the physical model using the Equation Editor is given in the Supplemental Information, Section 5.

5.5.2 Driftdiffusion Initial Conditions `dfic`

`dfic` defines the initial conditions to be used by `pdepe`. If running `equilibrate` to obtain the equilibrium solution or running `df` with an empty input solution, the first set of initial conditions are as described in Section 3.7. Otherwise, the final time point of the input solution is used.

5.5.3 Driftdiffusion Boundary Conditions `dfbc`

`dfbc` defines the system boundary conditions. The boundary condition expressions are passed to `pdepe` using two coefficients P and Q , with N_u elements, where N_u is the number of independent variables being solved for. The boundary conditions are expressed in the form:

```

182 %% Equation editor
183 % Time-dependence prefactor term
184 C_electron = 1;
185 C_hole = 1;
186 C_cation = 1;
187 C_potential = 0;
188 C = [C_electron; C_hole; C_cation; C_potential];
189
190 % Flux terms
191 F_electron = mue(i)*n*(-dVdx + gradEA(i)) + (Dn(i)*(dndx - ((n/Nc(i))*gradNc(i))));
192 F_hole = muh(i)*p*(dVdx - gradIP(i)) + (Dp(i)*(dpdx - ((p/Nv(i))*gradNv(i))));
193 F_cation = mucat(i)*(c*dVdx + kB*T*(dcdx + (c*(dcdx/(D0Scat(i)-c)))));
194 F_potential = (epp(i)/eppmax)*dVdx; % Poisson LHS
195 F = [mobset*F_electron; mobset*F_hole; K_cation*mobseti*F_cation; F_potential];
196
197 % Source terms
198 S_electron = g... % Generation
199 - radset*krad(i)*((n*p)-(ni(i)^2))... % Radiative recombination
200 - SRHset*(((n*p)-ni(i)^2)/((taun(i)*(p+pt(i)))+(taup(i)*(n+nt(i))))); % SRH recombination
201 S_hole = g... % Generation
202 - radset*krad(i)*((n*p)-(ni(i)^2))... % Radiative recombination
203 - SRHset*(((n*p)-ni(i)^2)/((taun(i)*(p+pt(i)))+(taup(i)*(n+nt(i))))); % SRH recombination
204 S_cation = 0;
205 S_potential = (q/(eppmax*epp0))*(-n+p-NA(i)+ND(i)-a+c+Nani(i)-Ncat(i)); % Poisson RHS
206 S = [S_electron; S_hole; S_cation; S_potential];

```

Listing 1 The Equation Editor. Coefficients that are defined at every position are indexed for the current x position using the index i . Gradient terms outside of the interfacial regions are equal to zero. This example does not include the expressions for anions. Location: `./Core/df - dfpde` subfunction.

```

338 % Left-hand boundary condition expressions
339 Pl = [mobset*(-sn_l*(ul(1) - nleft));
340       mobset*(-sp_l*(ul(2) - pleft));
341       0;
342       -ul(4)];
343 Ql = [1;
344       1;
345       1;
346       0];
347
348 % Right-hand boundary condition expressions
349 Pr = [mobset*(sn_r*(ur(1) - nright));
350       mobset*(sp_r*(ur(2) - pright));
351       0;
352       -ur(4)+Vbi-Vapp+Vres];
353 Qr = [1;
354       1;
355       1;
356       0];

```

Listing 2 Default boundary condition expressions for electrons, holes, cations and the electrostatic potential. Location: `./Core/df - dfbc` subfunction.

the code.

In addition to these subfunctions, `df` also calls two important external functions: the time mesh generator, `meshgen_t` and the function generator, `fun_gen`.

5.5.4 The time mesh generator `meshgen_t`.

`df` calls the time mesh generator `meshgen_t` at the start of the code. As discussed in Section 3.11, the solver uses an adaptive time step and interpolates the solution to the user-defined mesh. Hence the choice of mesh is not critical to time integration convergence. The values of the mesh should be chosen such as to resolve the solution properly on the appropriate timescales. The total time step of the solution `tmax` and the maximum time step (controlled using the `MaxStepFactor` property) do however influence convergence strongly. For this reason, where convergence is proving problematic it is recommended that either `tmax` or `MaxStepFactor` is reduced and the solution obtained in multiple steps.

5.5.5 The function generator `fun_gen`.

`df` calls `fun_gen` to generate time-dependent algebraic functions that define the applied voltage and light intensity conditions. `df` includes the ability to call two different light intensity functions with different light sources, enabling users to simulate a constant bias light and additional pump pulse using the square wave generator for example. Each function type requires a coefficients array with a number of

$$P(x, t, u) + Q(x, t) F \left(x, t, u, \frac{\partial u}{\partial x} \right) = 0. \quad (69)$$

For Dirichlet conditions P must be non-zero to define the variable values, whereas for Neumann conditions Q must be non-zero to define the flux density. Listing 2 shows how the default Driftfusion boundary conditions (described in Section 3.6) are implemented in the current version of

```

1 % Voltage function type
2 par.V_fun_type = 'sin';
3 % DC offset voltage (V)
4 par.V_fun_arg(1) = 0;
5 % AC voltage amplitude (V)
6 par.V_fun_arg(2) = 20e-3;
7 % Frequency (Hz)
8 par.V_fun_arg(3) = 1e3;
9 % Phase (Rads)
10 par.V_fun_arg(4) = 0;

```

Listing 3 Setting the function type and coefficients for the applied voltage function. Location: ./Scripts/Vapp_function_script.m.

elements determined by the function type and detailed in the comments of `fun_gen`. Listing 3 is an example from the `Vapp_function_script.m` script showing how to define a sine wave function for the applied voltage:

5.6 Solution structures

`df` outputs a solution structure `sol` with the following components:

- The solution matrix `u`: This is a three dimensional matrix for which the dimensions are (time, space, variable). The order of the variables are as follows:
 1. Electrostatic potential
 2. Electron density
 3. Hole density
 4. Cation density (where 1 mobile ionic carrier is stipulated)
 5. Anion density (where 2 mobile ionic carriers are stipulated)
- The spatial mesh `x`.
- The time mesh `t`.
- The parameters object `par`.

All other outputs can be calculated from the above by calling methods from `dfana`.

5.7 Calculating outputs: `dfana`

`dfana` is a collection of functions (methods) that enable the user to calculate outputs such as carrier currents, quasi-Fermi levels, recombination rates etc. from the solution matrix `u`, the parameters object `par` and the specified physical models. The use of a class in this instance enables the package syntax `dfana.my_calculation(sol)` to be used. For example the command:

```
[jdd, Jdd, xout] = dfana.Jddxt(sol),
```

outputs the individual carrier drift and diffusion fluxes and currents as two dimensional matrices which are elements of the structures `jdd` and `Jdd` respectively.² Many other examples of how `dfana` methods can be used to calculate outputs are given in the highlighted boxes of Section 3. The full list of available analysis methods can be obtained, and easily navigated to, by selecting the code in the MATLAB Current Folder window and opening the functions browser sub-window (see Supplemental Information, Figure S.20).

Users should note that, due to the computational cost of calling functions external to `df` with `pdepe`, the physical model described in the Equation Editor *is not coupled* to that used in the analysis functions. Users should take great care, therefore, when adapting the physics of the simulation to ensure that the model described in `dfana` is consistent with that in `df` (see Supplemental Information, Section 5.4 for further discussion).

5.8 Plotting the output: `dfplot`

`dfplot` is a class containing a collection of plotting methods. Similar to `dfana`, this enables the package syntax `dfplot.my_plot(sol)` to be used. For variables plotted as a function of position, an optional vector argument $[t_1, t_2, t_3, \dots, t_m]$ can be included to plot the solution at $t = t_1, t_2, t_3, \dots, t_m$, where m is the m th time point to be plotted. For example the command:

```
dfplot.Vx(sol, [0, 0.2, 0.4, 0.6, 0.8]);
```

plots the electrostatic component of the solution as a function of position at $t = 0, 0.2, 0.4, 0.6$, and 0.8 s as shown in Figure 13b. In this instance, as the scan rate was $k_{\text{scan}} = 1 \text{ V s}^{-1}$, these values also correspond to the applied voltage, as depicted. If no second argument is given then only the final time point is plotted. `dfplot` has been designed to allow users to easily create new plots by using the general two-dimensional property plotting function `dfplot.x2d`.

For variables plotted as a function of time the second argument defines the location. For example the command:

```
dfplot.Jt(sol, 1e-5);
```

plots the current density for each carrier as a function of position at $x = 10^{-5} \text{ cm}$. For plots where variables are integrated over a region of space, the second argument is a vector containing the limits $[x_1, x_2]$. Further details can be found in the comments of `dfplot`.

²Please note that due to the recalculation method the drift and diffusion currents presently do not cancel correctly - see Supplemental Information Section 8.4 for further details.

5.9 Getting started and the example scripts

While the underlying system may appear complex, Driftdiffusion has been designed to be user-friendly and with a few simple commands, users can simulate complex devices and transient optoelectronic experiment protocols. Table 2 is a full list of protocols available at the time of writing. In addition to the brief guide below, a quick start with up-to-date instructions can be found in the README.md file in the Driftdiffusion GitHub repository, and a series of sample scripts for running specific protocols are also presented in the /Scripts folder. New users are advised to study these scripts and adapt them to their own purposes.

5.9.1 How to build a device object, find the equilibrium solution and run a cyclic voltammogram

In this section some commonly-used commands are put together to show how to create a device object, obtain the equilibrium solutions for the device and run a protocol, in this example, simulating a cyclic voltammogram (CV). The doCV protocol applies a triangle voltage function to the device, with optional constant illumination, for a defined number of cycles enabling the device current-voltage characteristics at a given scan rate to be calculated. This has particular relevance to investigating hysteresis effects in PSCs for example.

At the start of each session, the system must be initialised by typing the command:

```
initialise_df;
```

To create a parameters object using the default parameters for a Spiro-OMeTAD/perovskite/TiO₂ perovskite solar cell the parameters class, pc is called with the file path to the appropriate .csv file as the input argument:

```
par = pc('Input_files/spiro_mapi_tio2.csv');
```

The equilibrium solutions with and without mobile ionic carriers for the device can now be obtained by calling the equilibrate protocol:

```
soleq = equilibrate(par);
```

As discussed in Section 5.3, the output structure soleq contains two solutions: soleq.el and soleq.ion. In this example we are interested in seeing how mobile ionic carriers influence the device currents so we will use the solution including mobile ionic charge carriers, soleq.ion.

To perform a cyclic voltammogram simulation from 0 to 1.2 to -0.2 to 0 V at 0.01 Vs⁻¹, under 1 sun illumination

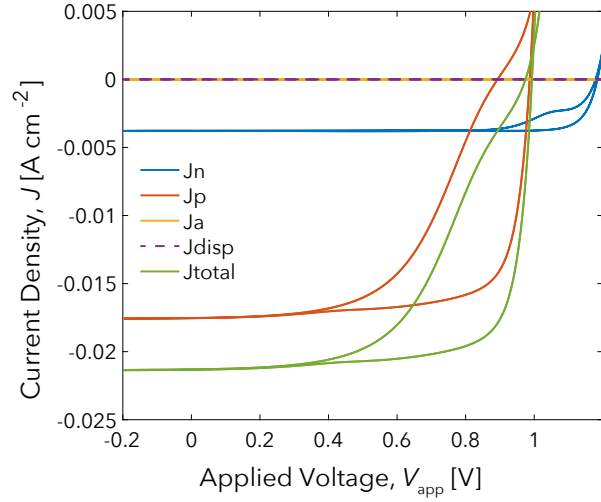


Fig. 17 Results obtained from the cyclic voltammogram (CV) protocol applied to the default Spiro-OMeTAD/perovskite/TiO₂ solar cell parameters. See the corresponding guide in Section 5.9.1 for step-by-step instructions on how to obtain these results and plot the figure.

we call the doCV protocol with the appropriate values for the arguments as detailed in the protocol comments as shown in Listing 4.

```
solcv = ...
doCV(soleq.ion, 1, 0, 1.2, -0.2, 50e-3, 2, 400);
```

Once a solution has been calculated the different components of the currents can be plotted as a function of voltage using the command:

```
dfplot.JVapp(solcv, par.d_midactive);
ylim([-25e-3, 5e-3]);
```

The second argument of dfplot.JVapp is the pre-calculated dependent property d_midactive, the value of which is equal to the position at the midpoint of the active layer of the device. The resulting plot is given in Figure 17 for reference.

5.9.2 How to change the physical model to consider the effect of photogenerated ionic carriers

A detailed step-by-step example of how to modify the physical model to account for the possible effects of photogenerated mobile ionic charge carriers is described in Section 5 of the Supplemental Information.


```

1 function sol_CV = doCV(sol_ini, light_intensity, VO, Vmax, Vmin, scan_rate, cycles, tpoints)
2 % Performs a cyclic voltammogram (CV) simulation
3 % Input arguments:
4 % SOL_INI = solution containing initial conditions
5 % LIGHT_INTENSITY = Light intensity for bias light (Suns)
6 % VO = Starting voltage (V)
7 % VMAX = Maximum voltage point (V)
8 % VMIN = Minimum voltage point (V)
9 % SCAN_RATE = Scan rate (Vs-1)
10 % CYCLES = No. of scan cycles
11 % TPOINTS = No. of points in output time array

```

Listing 4 First lines of the doCV protocol function. The input arguments for Driftfusion protocols are detailed in the comments at the start of each function. Location: ./Protocols/doCV.m .

5.10 Advanced features

5.10.1 Rebuilding device structures and spatial meshes: *refresh_device*

In some situations where device properties, such as layer widths, are changed in a user-defined script or function users may need to rebuild the device structures `dev` and `dev_ihalf`, and spatial meshes `x` and `x_ihalf`. To maintain code performance this is not performed automatically since non-device-related parameters are frequently changed within protocols. `meshgen_x` and `build_device` can be rerun and stored using the new parameter set ('refreshed') using the syntax:

```
par = refresh_device(par);
```

To further illustrate how to use `refresh_device`, `refresh_device_script`, a script describing the necessary steps to change the interfacial recombination parameters, is provided in the `Scripts` folder of the Driftfusion repository.

5.10.2 Parallel computing and parameter exploration: *explore*

Driftfusion's parameter exploration class `explore`, takes advantage of MATLAB's parallel computing toolbox, to enable multiple simulations to be calculated using a parallel pool. `explore_script.m` is an example script demonstrating how to use `explore` to run an active layer thickness versus light intensity parameter exploration and plot the outputs using `explore`'s embedded plotting tools.

6 Conclusions

We have developed an efficient and powerful tool for simulating semiconductor devices with mixed ionic-electronic conducting layers based on MATLAB's `pdepe` toolbox. The

default physical model of the simulator is based on well-established drift and diffusion principles. Distinct from existing codes Driftfusion can include up to two ionic carrier species in addition to electronic carriers, and virtually any number of material layers. This flexibility is made possible by a graded-interface approach in which the material properties of two adjoining semiconductor layers are mixed. This method has the further advantage of allowing interface specific properties to be specified.

Driftfusion was verified by comparing calculated solutions with two analytical and two existing numerical models which tested different aspects of the simulation. In all cases the agreement was good and the general device behaviour was reproduced. The unique treatment of the interfaces resulted in slight variations in the calculated currents as compared to other simulators using abrupt layer boundaries.

The system architecture was described in detail and the process by which users can define device properties and change the simulation's physical model were outlined. Protocol functions, which define time-dependent voltage and light conditions were described as well as the simulation solution structures and how to use built-in analysis and plotting functions to calculate and visualise outputs. A step-by-step guide was presented detailing how to create a device, find equilibrium solutions and calculate its current-voltage characteristics using a cyclic voltammogram protocol. Finally, advanced features, including how to calculate multiple solutions in parallel, were briefly introduced.

The ease with which the underlying models can be changed places Driftfusion in a unique space compared to other, similar, free-to-use simulations for which an intricate knowledge of the numerical mechanics is required to adapt the physical models.

Acknowledgements The authors would like to thank the UK Engineering and Physical Sciences Research Council for funding this work (Grant No. EP/J002305/1, No. EP/M025020/1, No. EP/M014797/1, No. EP/N020863/1, No. EP/R020574/1, No. EP/R023581/ 1, and No. EP/L016702/1). J.N. thanks the European Research Council for support under the European Unions Horizon 2020 research and innovation

program (grant agreement No. 742708). We would also like to thank: Emilio Palomares and Davide Moia for lending the expertise of their students to work on this project, and Diego Alonso Álvarez for his invaluable advice on preparing and improving the code.

Conflict of interest

The authors declare that they have no conflicts of interest.

References

1. Alonso-Álvarez D, Wilson T, Pearce P, Führer M, Farrell D, Ekins-Daukes N (2018) Solcore: a multi-scale, Python-based library for modelling solar cells and semiconductor materials. *Journal of Computational Electronics* 17:1099–1123, DOI 10.1007/s10825-018-1171-3, URL <https://doi.org/10.1007/s10825-018-1171-3>
2. Barnes PRF, Anderson AY, Durrant JR, O'Regan BC (2011) Simulation and measurement of complete dye sensitised solar cells: including the influence of trapping, electrolyte, oxidised dyes and light intensity on steady state and transient device behaviour. *Phys Chem Chem Phys* 13:5798–5816, DOI 10.1039/c0cp01554g
3. Belisle RA, Nguyen WH, Bowring AR, Calado P, Li X, Irvine SJC, McGehee MD, Barnes PRF, O'Regan BC (2016) Interpretation of inverted photocurrent transients in organic lead halide perovskite solar cells: proof of the field screening by mobile ions and determination of the space charge layer widths. *Energy & Environmental Science* 10(1):192–204, DOI 10.1039/C6EE02914K, URL <http://dx.doi.org/10.1039/C6EE02914K>
4. Bertoluzzi L, Boyd CC, Rolston N, Xu J, Prasanna R, O'Regan BC, McGehee MD (2019) Mobile Ion Concentration Measurement and Open-Access Band Diagram Simulation Platform for Halide Perovskite Solar Cells. *Joule* 4(1):109–127, DOI 10.1016/j.joule.2019.10.003, URL <https://doi.org/10.1016/j.joule.2019.10.003>
5. Burkhard GF, Hoke ET, McGehee MD (2010) Accounting for interference, scattering, and electrode absorption to make accurate internal quantum efficiency measurements in organic and other thin solar cells. *Advanced Materials* 22(30):3293–3297, DOI 10.1002/adma.201000883
6. Burkhard GF, Hoke ET, McGehee MD (2011) Transfer Matrix Optical Modeling. URL <https://web.stanford.edu/group/mcgehee/transfermatrix/>
7. Calado P (2017) Transient optoelectronic characterisation and simulation of perovskite solar cells. PhD thesis, Imperial College London, URL <https://spiral.imperial.ac.uk/handle/10044/1/66894>
8. Calado P, Telford AM, Bryant D, Li X, Nelson J, O'Regan BC, Barnes PR (2016) Evidence for ion migration in hybrid perovskite solar cells with minimal hysteresis. *Nature Communications* 7:13831, DOI 10.1038/ncomms13831, URL <http://www.nature.com/doi/10.1038/ncomms13831>
9. Calado P, Barnes PRF, Gelmetti I, Azzouzi M, Hilton B (2017) Driftdiffusion. DOI 10.5281/zenodo.3670155, URL <https://github.com/barnesgroupICL/Driftdiffusion>
10. Calado P, Burkitt D, Yao J, Troughton J, Watson TM, Carnie MJ, Telford AM, O'Regan BC, Nelson J, Barnes PR (2019) Identifying Dominant Recombination Mechanisms in Perovskite Solar Cells by Measuring the Transient Ideality Factor. *Physical Review Applied* 11(4):044005, DOI 10.1103/PhysRevApplied.11.044005, URL <https://link.aps.org/doi/10.1103/PhysRevApplied.11.044005>
11. COMSOL AB (2019) COMSOL Multiphysics
12. Courtier NE, Richardson G, Foster JM (2018) A fast and robust numerical scheme for solving models of charge carrier transport and ion vacancy motion in perovskite solar cells. *Applied Mathematical Modelling* 63:329–348, DOI 10.1016/j.apm.2018.06.051, URL <https://doi.org/10.1016/j.apm.2018.06.051>
13. Courtier NE, Cave JM, Foster JM, Walker AB, Richardson G (2019) How transport layer properties affect perovskite solar cell performance: insights from a coupled charge transport/ion migration model. *Energy & Environmental Science* 12(1):396–409, DOI 10.1039/C8EE01576G, URL <http://xlink.rsc.org/?DOI=C8EE01576G>
14. Courtier NE, Cave JM, Walker AB, Richardson G, Foster JM (2019) IonMonger: a free and fast planar perovskite solar cell simulator with coupled ion vacancy and charge carrier dynamics. *Journal of Computational Electronics* (0123456789), DOI 10.1007/s10825-019-01396-2, URL <https://doi.org/10.1007/s10825-019-01396-2>
15. Czaja P, Celino M, Giusepponi S, Gusso M, Aeberhard U (2017) Ab Initio Description of Optoelectronic Properties at Defective Interfaces in Solar Cells. In: Di Napoli E, Hermanns MA, Iliev H, Lintermann A, Peyser A (eds) *High-Performance Scientific Computing*, Springer International Publishing, Cham, pp 111–124
16. Eames C, Frost JM, Barnes PRF, O'Regan BC, Walsh A, Islam MS (2015) Ionic transport in hybrid lead iodide perovskite solar cells. *Nature Communications* 6:7497, DOI 10.1038/ncomms8497, URL <http://www.nature.com/doi/10.1038/>

- ncomms8497
17. Farrell P, Rotundo N, Doan DH, Kantner M, Fuhrmann J, Koprucki T (2016) Numerical methods for drift-diffusion models. Tech. rep., Leibniz-Institut im Forschungsverbund Berlin, Berlin
 18. Fluxim AG (2019) SETFOS: Semiconducting emissive thin film optics simulator
 19. Foster JM, Snaith HJ, Leijtens T, Richardson G (2014) A Model for the Operation of Perovskite Based Hybrid Solar Cells: Formulation, Analysis, and Comparison to Experiment. *Siam J Appl Math* 74(6):1935–1966, DOI 10.1137/130934258
 20. Haruyama J, Sodeyama K, Han L, Tateyama Y (2015) First-principles study of ion diffusion in perovskite solar cell sensitizers. *Journal of the American Chemical Society* 137(32):10048–10051, DOI 10.1021/jacs.5b03615
 21. Jacobs DA, Shen H, Pfeiffer F, Peng J, White TP, Beck FJ, Catchpole KR (2018) The two faces of capacitance: New interpretations for electrical impedance measurements of perovskite solar cells and their relation to hysteresis. *The Journal of Applied Physics* 124:225702, DOI 10.1063/1.5063259
 22. Kilic MS, Bazant MZ, Ajdari A (2007) Steric effects in the dynamics of electrolytes at large applied voltages. I. Double-layer charging. *Physical Review E - Statistical, Nonlinear, and Soft Matter Physics* 75(2):1–16, DOI 10.1103/PhysRevE.75.021502
 23. Minemoto T, Murata M (2014) Device modeling of perovskite solar cells based on structural similarity with thin film inorganic semiconductor solar cells. *Journal of Applied Physics* 116(5):054505, DOI 10.1063/1.4891982
 24. Minemoto T, Murata M (2015) Theoretical analysis on effect of band offsets in perovskite solar cells. *Solar Energy Materials and Solar Cells* 133:8–14, DOI 10.1016/j.solmat.2014.10.036, URL <http://dx.doi.org/10.1016/j.solmat.2014.10.036>
 25. Moia D, Gelmetti I, Calado P, Fisher W, Stringer M, Game O, Hu Y, Docampo P, Lidzey D, Palomares E, Nelson J, Barnes PRF (2019) Ionic-to-electronic current amplification in hybrid perovskite solar cells: ionically gated transistor-interface circuit model explains hysteresis and impedance of mixed conducting devices. *Energy Environ Sci* 12(4):1296–1308, DOI 10.1039/C8EE02362J, URL <http://dx.doi.org/10.1039/C8EE02362J>
 26. Nelson J (2003) *The physics of solar cells*. Imperial College Press
 27. Neukom MT, Züfle S, Knapp E, Makha M, Hany R, Ruhstaller B (2017) Why perovskite solar cells with high efficiency show small IV-curve hysteresis. *Solar Energy Materials and Solar Cells* 169:159–166, DOI 10.1016/j.solmat.2017.05.021
 28. Nie W, Tsai H, Asadpour R, Blancon Jc, Neukirch AJ, Gupta G, Crochet JJ, Chhowalla M, Tretiak S, Alam MA, Wang Hl, Mohite AD (2014) High-efficiency solution-processed perovskite solar cells with millimeter-scale grains. *Science* 347(6221):522 – 525, DOI 10.1126/science.aaa0472
 29. O’Kane SEJ, Richardson G, Pockett A, Niemann RG, Cave JM, Sakai N, Eperon GE, Snaith HJ, Foster JM, Cameron PJ, Walker AB (2017) Measurement and modelling of dark current decay transients in perovskite solar cells. *J Mater Chem C* 5(2):452–462, DOI 10.1039/C6TC04964H, URL <http://xlink.rsc.org/?DOI=C6TC04964H>
 30. van Reenen S, Kemerink M, Snaith HJ (2015) Modeling Anomalous Hysteresis in Perovskite Solar Cells. *The Journal of Physical Chemistry Letters* 6:3808–3814, DOI 10.1021/acs.jpclett.5b01645, URL <http://pubs.acs.org/doi/10.1021/acs.jpclett.5b01645>
 31. Richardson G, O’Kane SE, Niemann RG, Peltola TA, Foster JM, Cameron PJ, Walker AB (2016) Can slow-moving ions explain hysteresis in the current-voltage curves of perovskite solar cells? *Energy & Environmental Science* 9:1476–1485, DOI 10.1039/C5EE02740C, URL <http://pubs.rsc.org/en/content/articlelanding/2016/ee/c5ee02740c#!divAbstract>
 32. Shampine LF, Kierzenka J (2013) PDEPE
 33. Shockley W (1949) The Theory of pn Junctions in Semiconductors and pn Junction Transistors. *Bell Labs Technical Journal* 28(3):435–489, DOI 10.1002/j.1538-7305.1949.tb03645.x
 34. Shockley W, Read WT (1952) Statistics of the Recombination of Holes and Electrons. *Physical Review* 87(46):835–842, DOI 10.1103/PhysRev.87.835
 35. Skeel RD, Berzins M (1990) A Method for the Spatial Discretization of Parabolic Equations in One Space Variable. *SIAM Journal on Scientific and Statistical Computing* 11(1):1–32, DOI 10.1137/0911001, URL <http://epubs.siam.org/doi/abs/10.1137/0911001>
 36. Sze SM (1981) *Physics of semiconductor devices*, 2nd edn. John Wiley & Sons, Inc., New York
 37. Sze SM, Ng KK (2006) *Physics of semiconductor devices*. John Wiley & sons
 38. The Mathworks (2017) MATLAB
 39. Tress W (2012) *Device physics of organic solar cells*. PhD thesis, Dresden University of Technology
 40. Tress W, Marinova N, Moehl T, Zakeeruddin SM, Nazeeruddin MK, Grätzel M (2015) Understanding the rate-dependent JV hysteresis, slow time component, and aging in CH₃NH₃PbI₃ perovskite so-

- lar cells: the role of a compensated electric field. *Energy & Environmental Science* 8(3):995–1004, DOI 10.1039/C4EE03664F, URL <http://xlink.rsc.org/?DOI=C4EE03664F>
41. Van Roosbroeck W (1950) Theory of the Flow of Electrons and Holes in Germanium and Other Semiconductors. *Bell System Technical Journal* 29(4):560–607, DOI 10.1002/j.1538-7305.1950.tb03653.x
 42. Walsh A, Scanlon DO, Chen S, Gong XG, Wei Sh (2015) Self-Regulation Mechanism for Charged Point Defects in Hybrid. *Angewandte Chemie International Edition* 54:1791–1794, DOI 10.1002/anie.201409740
 43. Xiao Z, Yuan Y, Shao Y, Wang Q, Dong Q, Bi C, Sharma P, Gruverman A, Huang J (2014) Giant switchable photovoltaic effect in organometal trihalide perovskite devices. *Nature Materials* 14(February):193 – 198, DOI 10.1038/nmat4150, URL <https://www.nature.com/articles/nmat4150>
 44. Yang TY, Gregori G, Pellet N, Grätzel M, Maier J (2015) The Significance of Ion Conduction in a Hybrid Organic-Inorganic Lead-Iodide-Based Perovskite Photosensitizer. *Angewandte Chemie* 127:8016 –8021, DOI 10.1002/ange.201500014, URL <http://doi.wiley.com/10.1002/ange.201500014>
 45. Yang W, Yao Y, Wu CQ (2015) Origin of the high open circuit voltage in planar heterojunction perovskite solar cells: Role of the reduced bimolecular recombination. *Journal of Applied Physics* 117:095502, DOI 10.1063/1.4913519
 46. Zeghbroeck BV (2011) Principles of semiconductor devices, online edn. University of Colorado Boulder, Colorado Boulder
 47. Zeman M, van den Heuvel J, Kroon M, Willemsen J, Pieters B, Krc J, Solntsev S (2011) Advanced Semiconductor Analysis (ASA). URL <https://www.tudelft.nl/en/ewi/the-faculty/departments/electrical-sustainable-energy/photovoltaic-materials-and-devices/software-platform/asa-software/>

Supplemental information for Driftdfusion

An open source code for simulating ordered semiconductor devices with mixed ionic-electronic conducting materials

Philip Calado¹ · Ilario Gelmetti² · Benjamin Hilton¹ · Mohammed Azzouzi¹ · Jenny Nelson¹ · Piers R. F. Barnes¹

arXiv submission date: 9th September 2020

1 Universal constants, abbreviations and symbols

Table S.1 Universal constants.

Constant Name	Symbol	Driftdfusion Property Name	Value
Boltzmann constant	k_B	kB	$8.62 \times 10^{-5} \text{ eV K}^{-1}$
Charge of an electron	q	e	$1.60 \times 10^{-19} \text{ C}$
Permittivity of free space	ϵ_0	epp0	$8.85 \times 10^{-12} \text{ m}^{-3} \text{ kg}^{-1} \text{ s}^4 \text{ A}^2$

EPSRC grant Nos. EP/J002305/1, EP/M025020/1, EP/M014797/1, EP/R020574/1, EP/R023581/1, and EP/L016702/1

P. Calado

E-mail: p.calado13@imperial.ac.uk

¹ Department of Physics, Imperial College London, London SW7 2AZ, UK.

² Institute of Chemical Research of Catalonia (ICIQ), Barcelona Institute of Science and Technology (BIST), Avda. Paisos Catalans 16, 43007 Tarragona, Spain.

Table S.2 Table of symbols. †The absorption and photon flux data are loaded directly from libraries according to the layer names defined in `stack` and the choice of light source using the properties `light_source1` and `light_source2`. *Solely for the Methods-depletion-approximation branch. **For the .csv file the name thickness can also be used. For a complete description of all user-defined and dependent properties please see the comments in the parameters class `pc`. For information on calculated outputs see the analysis class `dfana`.

Symbol	Driftfusion Variable Name	Variable type	Name	Unit
α_{abs}	†	-	Absorption coefficient	cm^{-1}
γ	-	-	Reaction order	
ϵ_r	epp	Property	Relative permittivity	
η	-	-	External quantum efficiency	
κ	-	-	Reflectance	-
λ	-	-	Wavelength	nm
μ_e	mue	Property	Electron mobility	$\text{cm}^2 \text{V}^{-1} \text{s}^{-1}$
μ_h	muh	Property	Hole mobility	$\text{cm}^2 \text{V}^{-1} \text{s}^{-1}$
μ_a	muani	Property	Anion mobility	$\text{cm}^2 \text{V}^{-1} \text{s}^{-1}$
μ_c	mucat	Property	Cation mobility	$\text{cm}^2 \text{V}^{-1} \text{s}^{-1}$
ρ	rho	Calculated output	Charge density	cm^{-3}
σ	-	-	Conductivity	S cm
τ_n, SRH	taun	Property	SRH electron lifetime	s
τ_p, SRH	taup	Property	SRH hole lifetime	s
τ_n	taun*	Property	Electron first order lifetime	s
τ_p	taup*	Property	Hole first order lifetime	s
ϕ	†	-	Photon flux	$\text{cm}^{-2} \text{s}^{-1}$
Φ_{EA}	EA	Property	Electron affinity	eV
Φ_{IP}	IP	Property	Ionisation potential	eV
a	a	Solution variable	Mobile anion carrier density	cm^{-3}
a_{max}	amax	Property	Limiting anion density	cm^{-3}
c	c	Solution variable	Mobile cation carrier density	cm^{-3}
c_{max}	cmax	Property	Limiting cation density	cm^{-3}
d	d**	Property	Layer thickness	cm
d_{dev}	dcum(end)	Dependent property	Device thickness	cm
d_{DR}	-	-	Depletion region thickness	cm
g	gx1, gx2, gx	Property	Volumetric generation rate	$\text{cm}^{-3} \text{s}^{-1}$
g_0	g0	Property	Uniform generation rate	$\text{cm}^{-3} \text{s}^{-1}$
j	j	Calculated output	Flux density	$\text{cm}^{-2} \text{s}^{-1}$
k_γ	-	-	Rate coefficient for reaction order γ	Variable
B	krad	Property	Band-to-band recombination rate coefficient	$\text{cm}^{-3} \text{s}^{-1}$
k_{scan}	-	-	Current-voltage scan rate	Vs^{-1}
k_{TPV}	-	-	TPV decay rate coefficient	s^{-1}
n	n	Solution variable	Electron carrier density	cm^{-3}
n_0	n0	Dependent property	Equilibrium electron density	cm^{-3}
n_{id}	-	-	Diode ideality factor	
n_i	ni	Dependent property	Intrinsic carrier density	cm^{-3}
n_t	nt	Dependent property	SRH electron trap parameter	cm^{-3}
p	p	Solution variable	Hole carrier density	cm^{-3}
p_0	p0	Dependent property	Equilibrium hole density	cm^{-3}
p_t	pt	Dependent property	SRH hole trap parameter	cm^{-3}
r	r	Calculated output	Volumetric recombination rate	$\text{cm}^{-3} \text{s}^{-1}$
r_{btb}	r.btb	Calculated output	Band-to-band recombination rate	$\text{cm}^{-3} \text{s}^{-1}$
r_{SRH}	r.srh	Calculated output	SRH recombination rate	$\text{cm}^{-3} \text{s}^{-1}$
s_n	sn.l,sn.r	Property	Electron extraction/surface recombination coefficient	cm s^{-1}
s_p	sp.l,sp.r	Property	Hole extraction/surface recombination coefficient	cm s^{-1}
-	stack	Property	Materials layers names	-
t	t	Property	Time	s
w_n	-	-	n -type depletion width	cm
w_p	-	-	p -type depletion width	cm
x	x	Property	Position	cm
z	-	-	Generic carrier concentration	cm^{-3}

Table S.3 Table of symbols continued. For a complete description of all user-defined and dependent properties please see the comments in the parameters class `pc`. For information on calculated outputs see the analysis class `dfana`.

Symbol	Driftfusion Property Name	Variable type	Name	Unit
D_n	Dn	Solver variable	Electron diffusion coefficient	$\text{cm}^2 \text{s}^{-1}$
D_p	Dp	Solver variable	Hole diffusion coefficient	$\text{cm}^2 \text{s}^{-1}$
E	-	-	Energy	eV
E_γ	-	-	Photon energy	eV
E_{CB}	Ecb	Property	Conduction band energy	eV
E_{VB}	Evb	Property	Valence band energy	eV
E_{Fi}	Efi	Dependent property	Intrinsic Fermi energy	eV
E_{F0}	E0	Property	Equilibrium Fermi level	eV
E_{Fn}	Efn	Calculated output	Electron quasi Fermi level	eV
E_{Fp}	Efp	Calculated output	Hole quasi Fermi level	eV
E_{vac}	Evac	Calculated output	Vacuum energy	eV
E_g	Eg	Dependent property	Bandgap energy	eV
E_t	Et	Property	SRH trap energy	eV
F	F	Calculated output	Electric field	V cm^{-1}
J	J	Calculated output	Current density	A cm^{-2}
J_{SC}	Jsc	Calculated output	Short circuit current density	A cm^{-2}
J_0	-	-	Dark saturation current	A cm^{-2}
$J_{0,rad}$	-	-	Black body recombination current	A cm^{-2}
L	-	-	Diffusion length	cm
N_{ani}	Nani	Property	Intrinsic anion density	cm^{-3}
N_{cat}	Ncat	Property	Intrinsic cation density	cm^{-3}
N_A	NA	Dependent property	Acceptor density	cm^{-3}
N_D	ND	Dependent property	Donor density	cm^{-3}
N_{CB}	Ncb	Property	Conduction band effective density of states	cm^{-3}
N_{VB}	Nvb	Property	Valence band effective density of states	cm^{-3}
P	P	Calculated output	Power density	W cm^{-2}
Q	sigma	Calculated output	Integrated charge density	C cm^{-2}
R_S	-	-	Series resistance (area normalised)	Ωcm^2
S	-	-	Source/sink rate	$\text{cm}^{-3} \text{s}^{-1}$
T	T	Property	Temperature	K
T_S	-	-	Black body temperature	K
U_0	-	-	Black body recombination rate	$\text{cm}^{-3} \text{s}^{-1}$
V	V	Solution variable	Electrostatic potential	V
V_{app}	Vapp	Property	Applied potential	V
V_{bi}	Vbi	Dependent property	Built-in potential	V
V_{OC}	Voc	Calculated output	Open circuit voltage	V

Table S.4 Abbreviations.**General**

ASA	Advanced Semiconductor Analysis
AM	Air Mass
CB	Conduction Band
DD	Drift-Diffusion
DSSC	Dye Sensitised Solar Cell
eDOS	Effective density of states
EQE	External Quantum Efficiency
ETL	Electron Transport Layer
FF	Fill Factor
HTL	Hole transport Layer
<i>J-V</i>	Current density-Voltage Scan
LED	Light Emitting Diode
OPV	Organic Photovoltaic
PCE	Power Conversion Efficiency
PDEPE	Partial Differential Equation solver for Parabolic and Elliptic equations
PSC	Perovskite Solar Cell
PV	Photovoltaics
QFL	Quasi Fermi Level
SRH	Shockley-Read-Hall
VB	Valence Band

Materials

ITO	Indium tin oxide
MAPI	Methylammonium lead iodide
mp-TiO ₂	Mesoporous TiO ₂
PCBM	Phenyl-C61-butyric acid methyl ester
Spiro-OMeTAD	2,2',7,7'-Tetrakis[N,N-di(4-methoxyphenyl)amino]-9,9'-spirobifluorene

2 Energy level diagrams

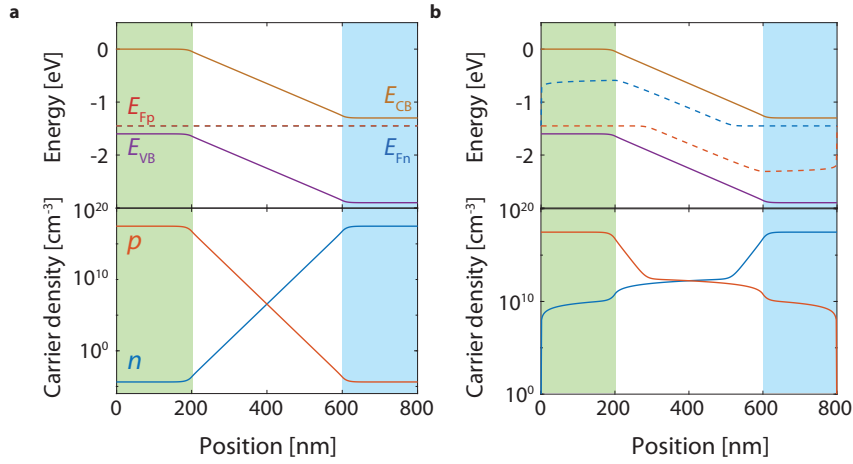


Fig. S.1 Short circuit equilibrium and illuminated p-i-n energy level diagrams and charge densities. (a) A simulated *p-i-n* structure at thermal equilibrium. p and n-type regions are shaded in green and blue respectively. The built-in field predominantly drops across the active layer (white region) while the chemical potential gradient is equal and opposite accounting for the same slope in the *n* and *p* profiles plotted on a logarithmic scale. This results in flat quasi-Fermi levels (QFLs) for both electrons and holes indicating that no current is flowing. (b) The same device under optical bias: The QFLs split due to population of the valence and conduction bands with photoexcited electrons and holes. Here, the Fermi level gradients indicate that net electron and hole currents are flowing in the device.

Energy level diagrams¹ provide a convenient method for graphing the spatial solution of the simulation at a given time. The electron and hole quasi-Fermi levels (QFLs), and conduction and valence band energies at each location within the device are plotted with respect to E_{vac} . The position of the QFLs with respect to the bands gives an indication of the occupation state of the bands, while the slope of the bands indicates the strength of the electric field. Figure S.1a and S.1b shows example energy level diagrams of a *p-i-n* structure at equilibrium and under illumination respectively.

¹The term ‘Band Diagrams’ is also often used interchangeably although we avoid this terminology here to prevent confusion with band structure diagrams.

3 Validation against existing models

The following sections provide references to the Github Driftdiffusion repository branch, parameters files and scripts required to reproduce the results in Section 4 of the Main Text.

3.1 The depletion approximation for a p-n junction

Repository branch: `Methods-depletion-approximation-comparison`

Parameters file: `./Input_files/TPV_test.csv`

Script: `df_methods_depletion_approx_pn_junction.m`

Table S.5 Key layer-specific parameters in the Driftdiffusion simulation comparison with the depletion approximation for a p-n junction.

Variable	Symbol	p-type quasi-neutral	p-type depletion region	n-type depletion region	n-type quasi-neutral	Unit
Thickness	d	10^{-2}	1.38×10^{-5}	6.25×10^{-5}	10^{-2}	cm
Electron affinity	Φ_{EA}	0	0	0	0	eV
Ionisation potential	Φ_{IP}	-1.12	-1.12	-1.12	-1.12	eV
Equilibrium Fermi energy	E_{F0}	-0.94	-0.94	-0.22	-0.22	eV
Acceptor density	N_A	2.01×10^{15}	2.01×10^{15}	0	0	cm ⁻³
Donor density	N_D	0	0	9.47×10^{15}	9.47×10^{15}	cm ⁻³
SRH trap energy	E_{trap}	-0.56	-0.56	-0.56	-0.56	eV
eDOS conduction band	N_{CB}	10^{19}	10^{19}	10^{19}	10^{19}	cm ⁻³
eDOS valence band	N_{VB}	10^{19}	10^{19}	10^{19}	10^{19}	cm ⁻³
Electron mobility	μ_e	2000	2000	2000	2000	cm ² V ⁻¹ s ⁻¹
Hole mobility	μ_h	2000	2000	2000	2000	cm ² V ⁻¹ s ⁻¹
Relative dielectric constant	ϵ_r	12	12	12	12	-
Uniform generation rate	g_0	0	3.49×10^{21}	3.49×10^{21}	0	cm ⁻³ s ⁻¹
First order recombination electron lifetime	τ_n	$10^{-6}, 10^{-7}, 10^{-8}$	10^{100}	10^{100}	10^{100}	s
First order recombination hole lifetime	τ_p	10^{100}	10^{100}	10^{100}	$10^{-6}, 10^{-7}, 10^{-8}$	s

Table S.6 Key device-wide parameters in the Driftdiffusion simulation comparison with the depletion approximation for a p-n junction.

Variable	Symbol	Unit
Left-hand boundary Fermi energy	Φ_{left}	-0.94 eV
Right-hand boundary Fermi energy	Φ_{right}	-0.22 eV
Left-hand boundary electron extraction coefficient	$s_{n,left}$	0 cm s ⁻¹
Right-hand boundary electron extraction coefficient	$s_{n,right}$	10^{10} cm s ⁻¹
Left-hand boundary hole extraction coefficient	$s_{p,left}$	10^{10} cm s ⁻¹
Right-hand boundary hole extraction coefficient	$s_{p,right}$	0 cm s ⁻¹

3.1.1 Additional data

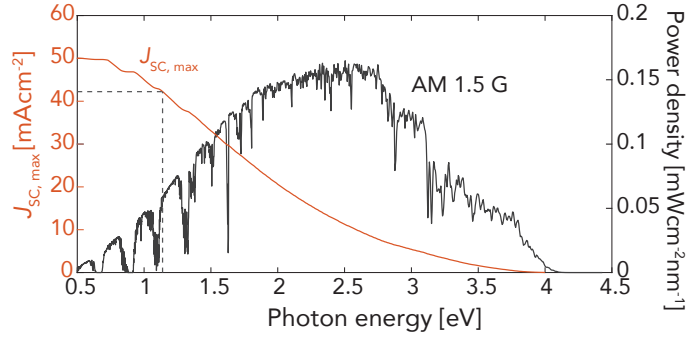


Fig. S.2 AM 1.5 solar spectrum and maximum theoretical short circuit current. AM 1.5 power density versus wavelength (right axis, black curve). Integrating the spectral photon flux above the band gap gives the maximum theoretical short circuit current $J_{SC,max}$ (left axis, red curve). The dashed line indicates the position of 1.12 eV. Note: 'Global Tilt' is for a south facing surface at an angle of 37 degrees to the horizontal and includes sky diffuse and diffuse reflected light from the ground.[5]

3.2 Transient photovoltage response of a single field-free device

Repository branch: `Methods`

Parameters file: `./Input_files/TPV_test.csv`

Script: `df_methods_TPV.m`

Table S.7 Key layer-specific parameters in the Driftfusion simulation comparison with transient photovoltage kinetic model analytical solution.

Variable	Symbol	Absorber layer	Unit
Thickness	d	10^{-5}	cm
Electron affinity	Φ_{EA}	-3.8	eV
Ionisation potential	Φ_{IP}	-5.4	eV
Equilibrium Fermi energy	E_{F0}	-4.6	eV
Acceptor density	N_A	0	cm^{-3}
Donor density	N_D	0	cm^{-3}
eDOS conduction band	N_{CB}	10^{20}	cm^{-3}
eDOS valence band	N_{VB}	10^{20}	cm^{-3}
Electron mobility	μ_e	10	$\text{cm}^2 \text{V}^{-1} \text{s}^{-1}$
Hole mobility	μ_h	10	$\text{cm}^2 \text{V}^{-1} \text{s}^{-1}$
Relative dielectric constant	ϵ_r	23	-
Uniform generation rate	g_0	1.89×10^{21}	$\text{cm}^{-3} \text{s}^{-1}$
Direct recombination coefficient	k_{rad}	10^{-10}	s

Table S.8 Key device-wide parameters in the Drift-diffusion simulation compared with transient photovoltage kinetic model analytical solution.

Variable	Symbol	Unit
Left-hand boundary Fermi energy	Φ_{left}	-4.6 eV
Right-hand boundary Fermi energy	Φ_{right}	-4.6 eV
Left-hand boundary electron extraction coefficient	$s_{n,left}$	0 cm s ⁻¹
Right-hand boundary electron extraction coefficient	$s_{n,right}$	0 cm s ⁻¹
Left-hand boundary hole extraction coefficient	$s_{p,left}$	0 cm s ⁻¹
Right-hand boundary hole extraction coefficient	$s_{p,right}$	0 cm s ⁻¹

3.2.1 Derivation of a zero-dimensional kinetic model of recombination

This section has been largely reproduced from reference [1].

Under the assumption that the parabolic band and Boltzmann approximations are valid,² the charge densities of electrons n and holes p for an intrinsic semiconductor with intrinsic carrier density n_i and Fermi energy E_{Fi} are given by:[4]

$$n = n_i \exp\left(\frac{E_{Fn} - E_{Fi}}{k_B T}\right) \quad (S.1)$$

$$p = n_i \exp\left(\frac{E_{Fi} - E_{Fp}}{k_B T}\right) \quad (S.2)$$

Using Equations S.1 and S.2, the open circuit (OC) voltage V_{OC} in a field free, zero-dimensional material, where electron and hole charge carrier concentrations are equal ($n = p$), can be expressed as:

$$V_{OC} = \frac{2k_B T}{q} \ln\left(\frac{n_{OC}}{n_i}\right) \quad (S.3)$$

Here, n_{OC} is carrier density at OC and is dependent on the generation rate g and the recombination model. For example, in an idealised device with band-to-band recombination only, the recombination rate r is given by $r = B(n^2 - n_i^2)$, where B is the band-to-band recombination coefficient. At OC steady-state, generation is equal to recombination ($r = g$) leading to:

$$n_{OC} = \left(\frac{g}{B} + n_i^2\right)^{1/2} \approx \left(\frac{g}{B}\right)^{1/2} \quad (S.4)$$

During a small perturbation measurement a small additional charge density $\Delta n \ll n_{OC}$ is injected into the device such that the state of the system is not significantly altered. In a transient photovoltage measurement this charge is generated by an excitation light pulse imposed onto a background bias light (Figure S.3a).

Figure S.3b is a schematic showing how the relaxation of the excess electron carrier density after a pulse results in a change in the electron quasi Fermi level (QFL). The recombination of excess charge with rate constant k_{rec} , results in an associated decay of the QFLs. In this 0-D representation, the open circuit voltage is defined by the difference in electron and hole QFLs ($qV_{OC} = E_{Fn} - E_{Fp}$) and decays with the same rate constant as the charge.

²Criteria for validity: the band edges can be modelled as parabolic functions and the quasi Fermi levels should be $> 3k_B T$ from their respective bands.[4]

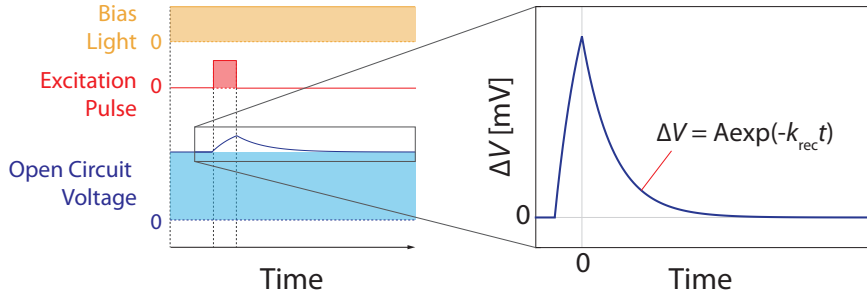


Fig. S.3 Transient photovoltaic experimental timeline The exponential decay rate constant of ΔV equates to k_{rec} in the 0-D model.

In the most general case, following a small perturbation ending at $t = 0$, the rate of change of addition charge $\frac{d\Delta n}{dt}$ can be expressed using a small perturbation rate constant, k_{TPV} (see reference [7] , pp. 101 – 103 for full derivation):

$$\frac{d\Delta n}{dt} \approx -k_{TPV} \Delta n \quad (S.5)$$

$$k_{TPV} = \sum_{ij} \left(k_{ij} n^{\gamma_i} p^{\gamma_j} \left(\frac{\gamma_i}{n} + \frac{\gamma_j}{p} \right) \right) \quad (S.6)$$

where i and j are summation indices and the exponents γ_i and γ_j can take any value (including non-integers). k_{ij} is the associated rate coefficient for the reaction order. The solution to Equation S.5 is an exponential:

$$\Delta n = \exp(-k_{TPV} t) \quad \text{for } t > 0 \quad (S.7)$$

Using Equation S.3, the change in open circuit voltage ΔV_{OC} produced by a light pulse introducing an additional charge Δn can be expressed as:

$$\Delta V_{OC} = \frac{2k_B T}{q} \ln \left(1 + \frac{\Delta n}{n_{OC}} \right) \approx \frac{2k_B T \Delta n}{n_{OC}}$$

Substituting for Δn using Equation S.7 leads to:

$$\Delta V_{OC} = \frac{2k_B T}{q n_{OC}} \exp(-k_{TPV} t) \quad \text{for } t > 0 \quad (S.8)$$

A similar method can be used to find the change in charge carrier density and voltage rise during a pulse of duration t_{pulse} :

$$\Delta n = \frac{\Delta g}{k_{TPV}} (1 - \exp(-k_{TPV}(t + t_{pulse}))) \quad \text{for } -t_{pulse} < t \leq 0 \quad (S.9)$$

$$\Delta V = \frac{2k_B T}{q n_{OC}} \frac{\Delta g}{k_{TPV}} (1 - \exp(-k_{TPV}(t + t_{pulse}))) \quad \text{for } -t_{pulse} < t \leq 0 \quad (S.10)$$

where Δg is the additional generation rate from the pulse light.

In experimental measurements, a single empirical reaction order γ , with the corresponding rate constant k_γ , is typically assumed to dominate recombination such that:

$$r = k_\gamma n^\gamma \quad (\text{S.11})$$

Accordingly, the slope of the $\log(k_{\text{TPV}})$ vs. $\log(n_{\text{OC}})$ plot can be used to determine γ :

$$\log(k_{\text{TPV}}) = (\gamma - 1)\log(n_{\text{OC}}) + \log(\gamma k_\gamma) \quad (\text{S.12})$$

3.3 Numerical solution for a three-layer devices without mobile ions: comparison with Advanced Semiconductor Analysis (ASA) software

Repository branch: `Methods`

Parameters files:

`./Input_files/3_layer_methods_test1a.csv`

`./Input_files/3_layer_methods_test1b.csv`

`./Input_files/3_layer_methods_test2a.csv`

`./Input_files/3_layer_methods_test2b.csv`

Script: `df_methods_ASA_comparison.m`

3.3.1 Parameter Sets 1a & 1b

Table S.9 Key layer-specific parameters for Parameter Sets 1a and 1b in the Driftfusion simulation comparison with ASA. HTL and ETL denote hole and electron transport layers respectively.

Variable	Symbol	HTL	Layer Absorber	ETL	Unit
Optical parameters material reference	-	SiO ₂	MAPICl	SiO ₂	-
Thickness	d	2×10^{-5}	(a) 4×10^{-5} (b) 2×10^{-5}	0.5×10^{-5}	cm
Electron affinity	Φ_{EA}	-3.3	-3.8	-4.0	eV
Ionisation potential	Φ_{IP}	-5.3	-5.4	-6.2	eV
Equilibrium Fermi energy	E_{F0}	-5.2	-4.6	-4.15	eV
Acceptor density	N_A	2.09×10^{17}	0	0	cm ⁻³
Donor density	N_D	0	0	3.02×10^{16}	cm ⁻³
SRH trap energy	E_{trap}	-4.3	-4.6	-5.1	eV
eDOS conduction band	N_{CB}	10^{19}	10^{18}	10^{19}	cm ⁻³
eDOS valence band	N_{VB}	10^{19}	10^{18}	10^{19}	cm ⁻³
Electron mobility	μ_e	0.2	20	0.1	cm ² V ⁻¹ s ⁻¹
Hole mobility	μ_h	0.02	20	0.01	cm ² V ⁻¹ s ⁻¹
Relative dielectric constant	ϵ_r	4	23	12	-
SRH recombination electron lifetime	τ_n	10^{-8}	10^{-7}	10^{-9}	s
SRH recombination hole lifetime	τ_p	10^{-8}	10^{-7}	10^{-9}	s

Table S.10 Key device-wide parameters for Parameter Sets 1a and 1b in the Driftdiffusion simulation comparison with ASA.

Variable	Symbol	Unit
Left-hand boundary Fermi energy	Φ_{left}	-5.2 eV
Right-hand boundary Fermi energy	Φ_{right}	-4.15 eV
Left-hand boundary electron extraction coefficient	$s_{n,left}$	10^8 cm s ⁻¹
Right-hand boundary electron extraction coefficient	$s_{n,right}$	10^8 cm s ⁻¹
Left-hand boundary hole extraction coefficient	$s_{p,left}$	10^8 cm s ⁻¹
Right-hand boundary hole extraction coefficient	$s_{p,right}$	10^8 cm s ⁻¹

3.3.2 Parameter Sets 2a & 2b

Table S.11 Key layer-specific parameters for Parameter Sets 2a and 2b in the Driftdiffusion simulation comparison with ASA. HTL and ETL denote hole and electron transport layers respectively.

Variable	Symbol	HTL	Layer Absorber	ETL	Unit
Optical parameters material reference	-	SiO ₂	MAPICl	SiO ₂	-
Thickness	d	1×10^{-5}	2×10^{-5}	0.7×10^{-5}	cm
Electron affinity	Φ_{EA}	-3.0	-3.8	-4.1	eV
Ionisation potential	Φ_{IP}	-5.1	-5.2	-6.2	eV
Equilibrium Fermi energy	E_{F0}	-5.0	-4.6	-4.4	eV
Acceptor density	N_A	2.09×10^{17}	8.32×10^7	0	cm ⁻³
Donor density	N_D	0	0	9.12×10^{14}	cm ⁻³
SRH trap energy	E_{trap}	-4.05	-4.5	-5.15	eV
eDOS conduction band	N_{CB}	(a) 10^{19} (b) 10^{18}	10^{18}	(a) 10^{20} (b) 10^{18}	cm ⁻³
eDOS valence band	N_{VB}	(a) 10^{19} (b) 10^{18}	10^{18}	(a) 10^{20} (b) 10^{18}	cm ⁻³
Electron mobility	μ_e	0.2	20	0.1	cm ² V ⁻¹ s ⁻¹
Hole mobility	μ_h	0.02	2	0.001	cm ² V ⁻¹ s ⁻¹
Relative dielectric constant	ϵ_r	8	10	20	-
SRH recombination electron lifetime	τ_n	10^{-9}	10^{-7}	10^{-6}	s
SRH recombination hole lifetime	τ_p	10^{-9}	10^{-7}	10^{-6}	s

Table S.12 Key device-wide parameters for Parameter Sets 2a and 2b in the Driftfusion simulation comparison with ASA.

Variable	Symbol	Unit
Left-hand boundary Fermi energy	Φ_{left}	−5.0 eV
Right-hand boundary Fermi energy	Φ_{right}	−4.4 eV
Left-hand boundary electron extraction coefficient	$s_{n,left}$	10^8 cm s ^{−1}
Right-hand boundary electron extraction coefficient	$s_{n,right}$	10^8 cm s ^{−1}
Left-hand boundary hole extraction coefficient	$s_{p,left}$	10^8 cm s ^{−1}
Right-hand boundary hole extraction coefficient	$s_{p,right}$	10^8 cm s ^{−1}

3.3.3 Beer Lambert generation profile as a function of wavelength

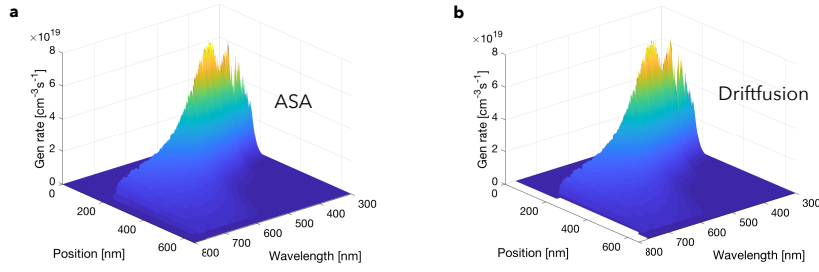


Fig. S.4 Comparison of optical generation rate as a function of wavelength and position using the Beer-Lambert model calculated by Driftdiffusion and ASA.

3.3.4 Equilibrium states

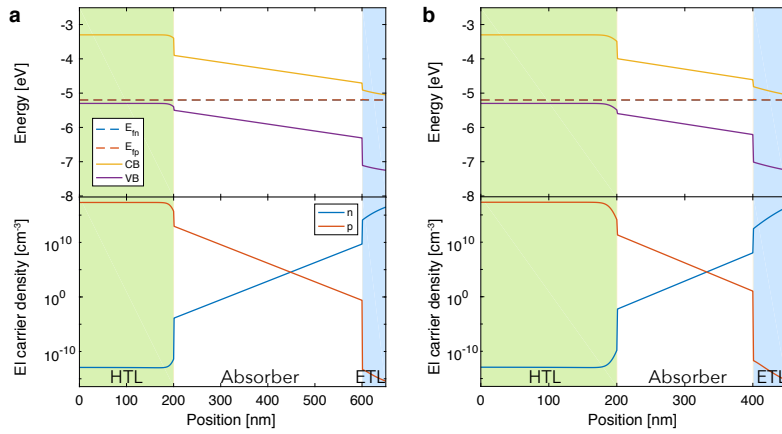


Fig. S.5 Equilibrium energy level diagrams and carrier densities for Parameter Sets 1a and 1b. Equilibrium states for (a) Parameter Set 1a and (b) Parameter Set 1b.

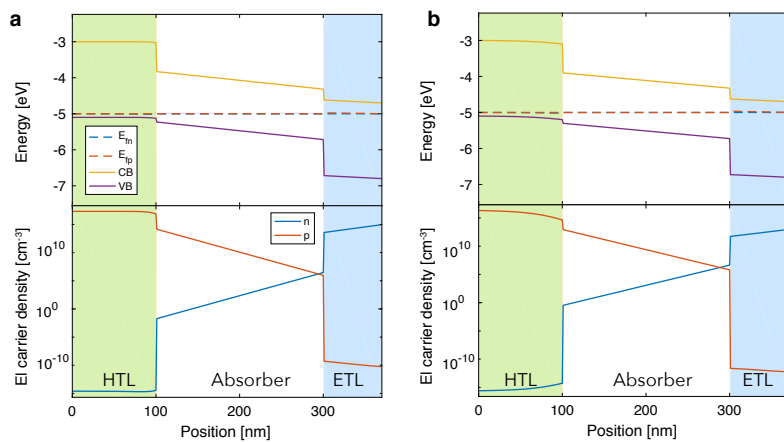


Fig. S.6 Equilibrium energy level diagrams and carrier densities for Parameter Sets 2a and 2b. Equilibrium states for (a) Parameter Set 2a and (b) Parameter Set 2b.

3.3.5 Additional data

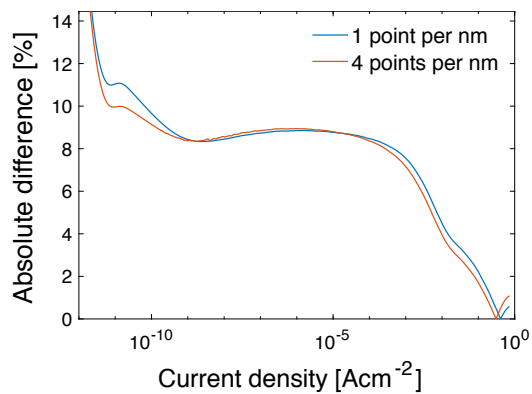


Fig. S.7 Absolute difference between dark current obtained using Driftfusion and ASA for different point spacings in ASA for Parameter Set 2.

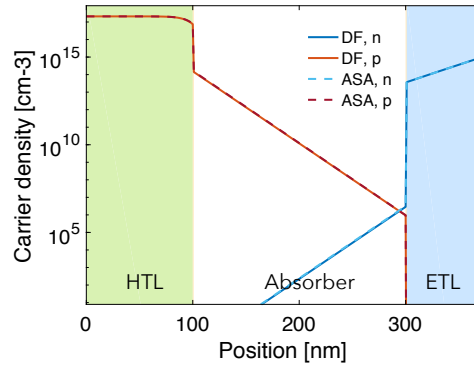


Fig. S.8 Carrier densities at equilibrium for a simulated device comparing Driftfusion with ASA using parameter set 2. Results from Driftfusion are indicated by solid curves whereas results from ASA are indicated by dashed curves.

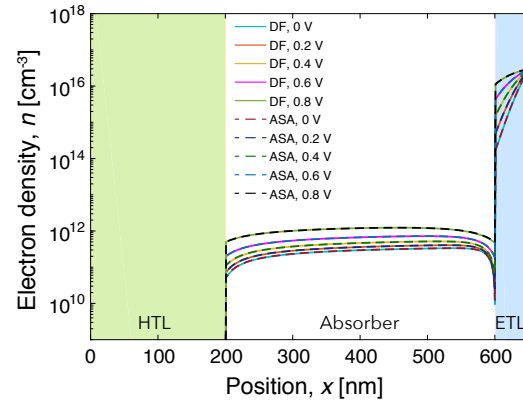


Fig. S.9 Comparison of calculated Driftfusion and ASA electron density profiles during J - V scan for a three-layer device with Parameter Set 1 under illumination.

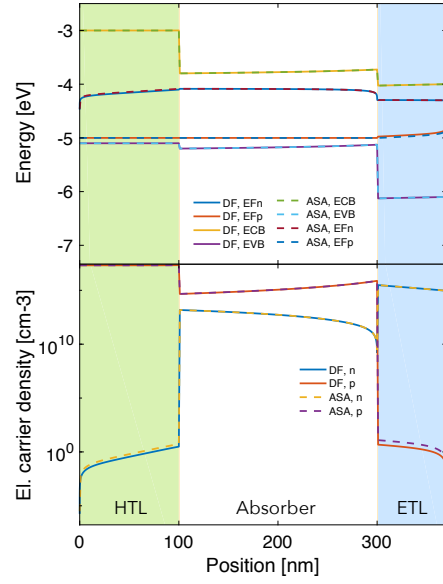


Fig. S.10 Energy level diagram and carrier densities for a device with properties defined by Parameter Set 2 under illumination at $V_{app} = 0.7$ V. Results from Driftfusion indicated by the solid lines, while those from ASA are indicated by dashed lines.

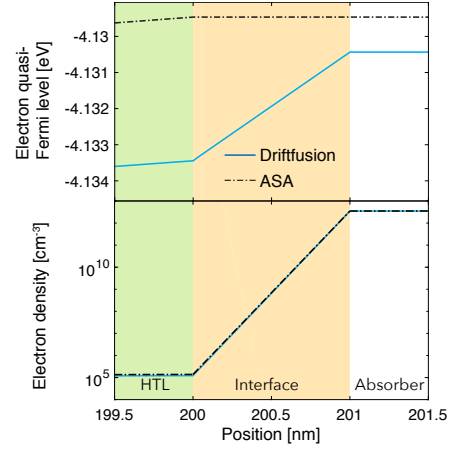


Fig. S.11 Electron quasi-Fermi level and carrier density under illumination at $V_{app} = 1$ V comparison between Driftfusion and ASA. Results from Driftfusion are indicated by solid blue curves whereas results from ASA are indicated by dashed black curves.

3.4 Numerical solution for a three-layer device with mobile ions: comparison with IonMonger

Repository branch: `Methods_IonMonger_comparison`

Parameters files: `./Input_files/IonMonger_default_noIR.csv`

Script: `df_methods_IonMonger_comparison`

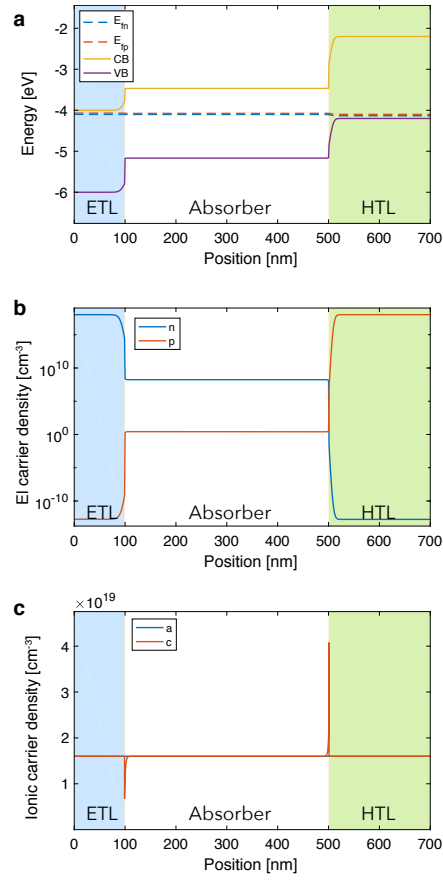
Table S.13 Key layer-specific parameters for simulation comparison with IonMonger. *Ions in these layer are immobile and are balanced by a static counter charge hence they do not contribute to mobile ionic space charge. [†]The limiting ion densities have been set to a very high value since IonMonger does not include a steric model similar to that described in Section 3.4. [‡] Minority carriers are not simulated in the transport layers in IonMonger, hence recombination was effectively switched off in these regions. HTL and ETL denote hole and electron transport layers respectively.

Variable	Symbol	HTL	Layer Absorber	ETL	Unit
Optical parameters material reference	-	SiO ₂	MAPICl	SiO ₂	-
Thickness	d	1×10^{-5}	4×10^{-5}	2×10^{-5}	cm
Electron affinity	Φ_{EA}	-3.1	-3.7	-4.0	eV
Ionisation potential	Φ_{IP}	-5.1	-5.4	-6.0	eV
Equilibrium Fermi energy	E_{F0}	-5.0	-4.55	-4.1	eV
Acceptor density	N_A	1.03×10^{18}	8.32×10^7	0	cm ⁻³
Donor density	N_D	0	0	1.03×10^{18}	cm ⁻³
SRH trap energy	E_{trap}	-4.1	-4.55	-5.0	eV
eDOS conduction band	N_{CB}	5×10^{19}	8.1×10^{18}	5×10^{19}	cm ⁻³
eDOS valence band	N_{VB}	5×10^{19}	5.8×10^{18}	5×10^{19}	cm ⁻³
Intrinsic cation density	N_{cat}	$5 \times 10^{19*}$	5×10^{19}	$5 \times 10^{19*}$	cm ⁻³
Intrinsic anion density	N_{ani}	$5 \times 10^{19*}$	$5 \times 10^{19*}$	$5 \times 10^{19*}$	cm ⁻³
Limiting cation density	c_{max}	$10^{100†}$	$10^{100†}$	$10^{100†}$	cm ⁻³
Limiting anion density	a_{max}	$10^{100†}$	$10^{100†}$	$10^{100†}$	cm ⁻³
Electron mobility	μ_e	0.2	20	0.1	cm ² V ⁻¹ s ⁻¹
Hole mobility	μ_h	0.02	2	0.001	cm ² V ⁻¹ s ⁻¹
Cation mobility	μ_c	0 [‡]	3.12×10^{-12}	0 [‡]	cm ² V ⁻¹ s ⁻¹
Anion mobility	μ_a	0 [‡]	0 [‡]	0 [‡]	cm ² V ⁻¹ s ⁻¹
Relative dielectric constant	ϵ_r	3	24.1	10	-
Direct recombination coefficient	k_{rad}	0 [‡]	1×10^{-12}	0 [‡]	cm ³ s ⁻¹
SRH recombination electron lifetime	τ_n	$10^{100‡}$	3×10^{-10}	$10^{100‡}$	s
SRH recombination hole lifetime	τ_p	$10^{100‡}$	3×10^{-8}	$10^{100‡}$	s

Table S.14 Key device-wide parameters for simulation comparison with IonMonger.

Variable	Symbol	Unit
Left-hand boundary Fermi energy	Φ_{left}	-4.1 eV
Right-hand boundary Fermi energy	Φ_{right}	-5.0 eV
Left-hand boundary electron extraction coefficient	$s_{n,left}$	10^7 cm s ⁻¹
Right-hand boundary electron extraction coefficient	$s_{n,right}$	0 cm s ⁻¹
Left-hand boundary hole extraction coefficient	$s_{p,left}$	0 cm s ⁻¹
Right-hand boundary hole extraction coefficient	$s_{p,right}$	10^7 cm s ⁻¹

3.4.1 Equilibrium state

**Fig. S.12** Equilibrium energy level diagrams and carrier densities for the IonMonger comparison.

3.4.2 Additional data

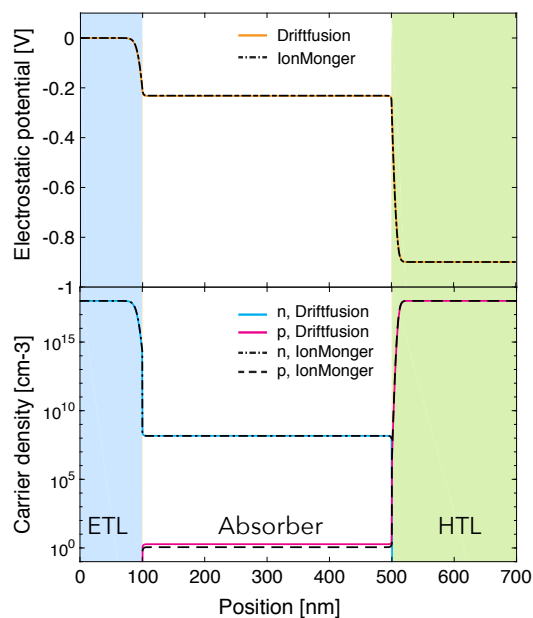


Fig. S.13 Comparison of the equilibrium state electrostatic potential and electronic carrier densities of the simulated device calculated by Driftdiffusion and IonMonger. Results from Driftdiffusion (DF) are indicated by solid coloured lines, whereas those from IonMonger (IM) are indicated by dashed black lines.

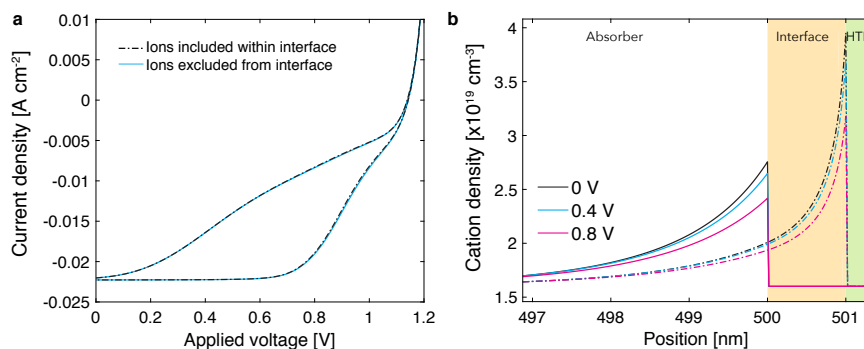


Fig. S.14 Comparison of current voltage characteristics and ionic carrier density profiles for a three-layer device calculated with Driftdiffusion. (a) Current-voltage scans for the three-layer device described by the parameters given in Tables S.13 and S.14 at a scan rate of 1 V s^{-1} . (b) Corresponding ionic carrier densities for the two conditions at increasing applied voltage. Solid lines indicate calculations where ions were excluded, whilst dashed lines indicate cases where ions were included in the interface regions (yellow background). The green background indicates the hole transport layer.

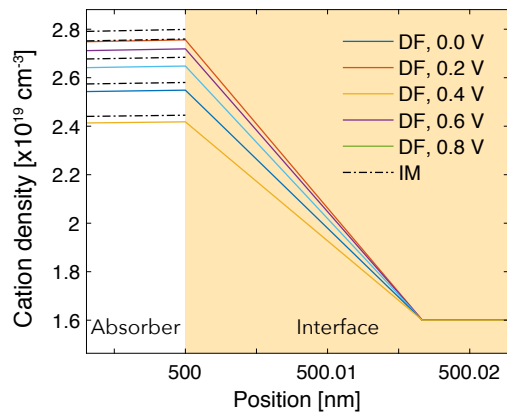


Fig. S.15 Zoom of ionic carrier density profiles for a three-layer device calculated with Driftfusion. Results from Driftfusion (DF) are indicated by solid coloured lines, whereas those from IonMonger (IM) are indicated by dashed black lines.

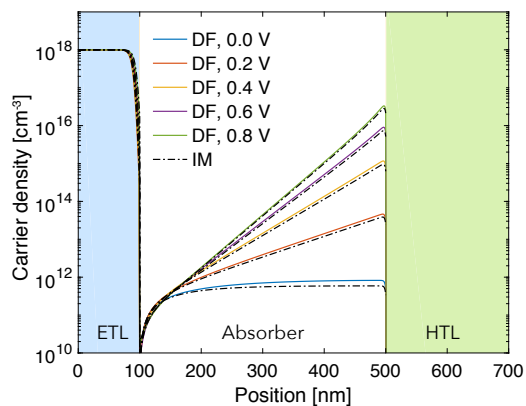


Fig. S.16 Comparison of electron densities during a current-voltage scan for a three-layer device calculated with Driftfusion and IonMonger. Results from Driftfusion (DF) are indicated by solid coloured lines, whereas those from IonMonger (IM) are indicated by dashed black lines.

4 System architecture

4.1 Creating the generation profile

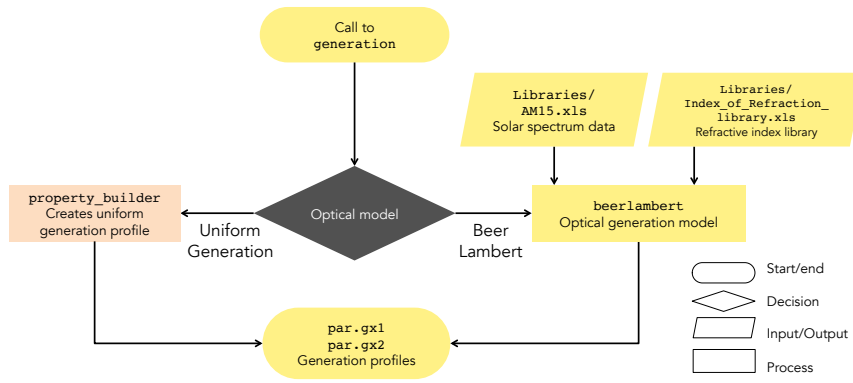


Fig. S.17 Flow diagram for building the generation profile.

5 Using the equation editor to adapt the physical model: Example

In the current version of Driftdusion the integrated density of ions in the device is constant in time i.e. ionic carriers do not have generation and recombination terms. In the following example generation and recombination terms proportional to the generation rate are added using the equation editor.

5.1 Switching to two ionic carrier species

We start with the default expressions shown in Listing 1 of the Main Text and the input properties defined in `Input_files/spiro_mapitio2.csv`. To ensure charge conservation we maintain ionic carrier neutrality, two ionic carrier variables are required. As such we first need to set `N_ionic_species` to 2 in the `.csv` file as shown in Figure S.18

sn_l	sn_r	sp_l	sp_r	PhiA	PhiC	OM	xmesh_type	side	N_ionic_species
1.00E+07	1.00E+07	1.00E+07	1.00E+07	-4.80E+00	-4.20E+00	1.00E+00	5.00E+00	2.00E+00	2

Fig. S.18 Setting the number of ionic carrier variables to 2.

5.2 Adding new device properties

In order to be able to adjust our generation term we will introduce two new device properties `k_iongen` and `k_ionrec` that characterise the ionic generation and recombination rates respectively. We will assume that these terms are material specific and equal to zero in the transport layers of our three-layer device. These rate coefficients need to be added as arrays to the parameters class `pc` and the device builder before we can create the parameters object for the device. First we create the properties in `pc` with default values as shown in Listing S1.

```

144     %% Mobile ions
145     % Mobile ion defect density [cm-3]
146     N_ionic_species = 1;
147     K_anion = 1;          % Coefficients to easily accelerate ions
148     K_cation = 1;         % Coefficients to easily accelerate ions
149     Nani = [1e19];
150     Ncat = [1e19];
151     % Approximate density of iodide sites [cm-3]
152     % Limits the density of iodide vancancies
153     DOSani = [1.21e22];
154     DOScat = [1.21e22];
155     % Ionic generation and recombination rates
156     k_iongen = [0];
157     k_ionrec = [0];

```

Listing 1 Creating property arrays in the parameters class. New coefficients for ionic generation and recombination coefficients are added in lines 156 and 157.

Listing S2 shows how new properties can then be added to the device builder. The new coefficient arrays `k_iongen` and `k_ionrec` are used as the first input arguments. Device builder then uses these values with the interface grading option to define the values of these

properties at every point in the device and stores the resulting arrays in the device structures `par.dev` and `par.dev_ihalf`. Here the 'lin_graded' option is chosen to linearly grade the new properties in the interface/junction regions.

```

1 function dev = build_device(par, meshoption)
2 % BUILD_DEVICE calls BUILD_PROPERTY for each device property. BUILD_PROPERTY
   then defines the
3 % properties at each point on the grid defined by MESHOPTION
4
5 switch meshoption
6     case 'iwhole'
7         xmesh = par.xx;
8     case 'ihalf'
9         xmesh = getvarihalf(par.xx);
10 end
11
12 % Properties with constant values in the interfacial regions
13 dev.taun = build_property(par.taun, xmesh, par, 'constant', 0);
14 dev.taup = build_property(par.taup, xmesh, par, 'constant', 0);
15 dev.k_iongen = build_property(par.k_iongen, xmesh, par, 'constant', 0);
16 dev.k_ionrec = build_property(par.k_ionrec, xmesh, par, 'constant', 0);
17
18 % Linearly graded properties
19 dev.EA = build_property(par.EA, xmesh, par, 'lin_graded', 0);
20 dev.IP = build_property(par.IP, xmesh, par, 'lin_graded', 0);
21 dev.mue = build_property(par.mue, xmesh, par, 'lin_graded', 0);
22 dev.muh = build_property(par.muh, xmesh, par, 'lin_graded', 0);
23 dev.mucut = build_property(par.mucut, xmesh, par, 'lin_graded', 0);
24 dev.muani = build_property(par.muani, xmesh, par, 'lin_graded', 0);
25 dev.epp = build_property(par.epp, xmesh, par, 'lin_graded', 0);
26 dev.krad = build_property(par.krad, xmesh, par, 'lin_graded', 0);
27 dev.E0 = build_property(par.E0, xmesh, par, 'lin_graded', 0);
28 dev.Et = build_property(par.Et, xmesh, par, 'lin_graded', 0);

```

Listing 2 Adding properties to the device builder.

Once the new properties have been added to the `pc` and `build_device`, they can additionally be added to the `.csv` parameters file and `import_properties` to enable them to be easily imported. Figure S.19 shows two new columns added to the `.csv` file defining `k_iongen` and `k_ionrec` for each layer.

L	M	N	O	P	Q	R	S	T	U	V	W	X	Y	Z
Ncat	Nani	DOScat	DOSani	mue	muh	mucut	muani	epp	g0	krad	taun	taup	k_iongen	k_ionrec
1.00E+18	1.00E+18	1.21E+22	1.21E+22	0.02	0.02	0.00E+00	0.00E+00	4.00E+00	0.00E+00	3.18E-11	1.00E-06	1.00E-06	0.00E+00	0.00E+00
1.00E+18	1.00E+18	1.21E+22	1.21E+22	2.00E+01	2.00E+01	1.00E-10	1.00E-10	2.30E+01	2.64E+21	3.60E-12	1.00E-07	1.00E-07	1.00E-03	1.00E+00
1.00E+18	1.00E+18	1.21E+22	1.21E+22	1.00E-01	1.00E-01	0.00E+00	0.00E+00	1.20E+01	0.00E+00	1.54E-10	1.00E-06	1.00E-06	0.00E+00	0.00E+00

Fig. S.19 Adding new properties to the `.csv` file. The new properties `k_iongen` and `k_ionrec` have been added to the final two columns.

New properties can be inserted anywhere the user chooses into the table as `import_properties` checks for matches between the column headers and listed property names. Lastly, the new properties are added to `import_properties` using try statements (Listing 3). If a match to a column heading is found in the `.csv` file the the properties are imported, otherwise the default values in `pc` are used.

```

182 try
183     par.k_iongen = T{1, 'k_iongen'};
184 catch
185     warning('k_iongen undefined in .csv. Using default in PC')

```

```

186 end
187 try
188     par.k_ionrec = T{1, 'k_ionrec'};
189 catch
190     warning('k_ionrec undefined in .csv. Using default in PC')
191 end

```

Listing 3 Including new properties to be imported from the .csv file in import_properties.

5.3 Using the equation editor

For simplicity, we will assume that ionic carriers are generated at a rate proportional to the optical intensity and hence the electron and hole generation rate g . We will further assume that the ionic carriers recombine at a rate proportional to their respective densities. We stress here that there is no physical basis for this choice of models and they are only been used for illustrative purposes. To adapt the Driftdiffusion master code `df` to our purposes we first need to unpack the new variables from the parameters object by adding the to the list of variables at the start of the code as shown in Listing S4.

```

113 %% Generation
114 g1_fun = fun_gen(par.g1_fun_type);
115 g2_fun = fun_gen(par.g2_fun_type);
116 gxt1 = 0;
117 gxt2 = 0;
118 g = 0;
119 gx1 = par.gx1;
120 gx2 = par.gx2;
121 int1 = par.int1;
122 int2 = par.int2;
123 g1_fun_type = par.g1_fun_type;
124 g2_fun_type = par.g2_fun_type;
125 g1_fun_arg = par.g1_fun_arg;
126 g2_fun_arg = par.g2_fun_arg;
127 k_iongen = device.k_iongen;
128 k_ionrec = device.k_ionrec;

```

Listing 4 Unpacking the new coefficients at the start of `df`.

While this approach appears laborious, creating individual variables in the workspace in this way (as opposed to using `par.k_iongen` directly in the Equation Editor for example) dramatically improves the performance of the code.

These terms are then simply added to the appropriate lines in the Equation Editor as shown in Listing S5

```

184 %% Equation editor
185 % Time-dependence prefactor term
186 C_electron = 1;
187 C_hole = 1;
188 C_cation = 1;
189 C_potential = 0;
190 C = [C_electron; C_hole; C_cation; C_potential];
191
192 % Flux terms
193 F_electron = mue(i)*n*(-dVdx+gradEA(i))+(Dn(i)*(dndx-((n/Nc(i))*gradNc(i))));
194 F_hole = muh(i)*p*(dVdx-gradIP(i))+(Dp(i)*(dpdx-((p/Nv(i))*gradNv(i))));
195 F_cation = mucat(i)*(c*dVdx+kB*T*(dcdx+(c*(dcdx/(D0Scat(i)-c)))));
196 F_potential = (epp(i)/eppmax)*dVdx;

```

```

197 F = [mobset*F_electron; mobset*F_hole; K_cation*mobseti*(F_cation);
      F_potential];
198
199 % Source terms
200 S_electron = g - radset*krad(i)*((n*p)-(ni(i)^2))...
201   - SRHset(((n*p)-ni(i)^2)/((taun(i)*(p+pt(i)))+(taup(i)*(n+nt(i)))));
202 S_hole = g - radset*krad(i)*((n*p)-(ni(i)^2))...
203   - SRHset(((n*p)-ni(i)^2)/((taun(i)*(p+pt(i)))+(taup(i)*(n+nt(i)))));
204 % New source term for cations
205 S_cation = k_iongen*g - k_ionrec*(c*a-Ncat(i)*Nani(i));
206 S_potential = (q/(eppmax*epp0))*(-n+p-NA(i)+ND(i)-a+c-Ncat(i)*Nani(i));
207 S = [S_electron; S_hole; S_cation; S_potential];

```

Listing 5 Adding source terms for ionic carriers in the Equation Editor. New terms for generation and recombination of cations are introduced on line 205.

5.4 Adapting analysis functions in dfana to the new physical model

It is particularly important to remember that the physical models in the master code and the analysis functions are not coupled. We therefore need to adapt any of the analysis functions in `dfana` to account for changes to the physical model. For example if one were to change the recombination model, `dfana.calcU` would need to be updated to account for this.

6 Browsing available class methods

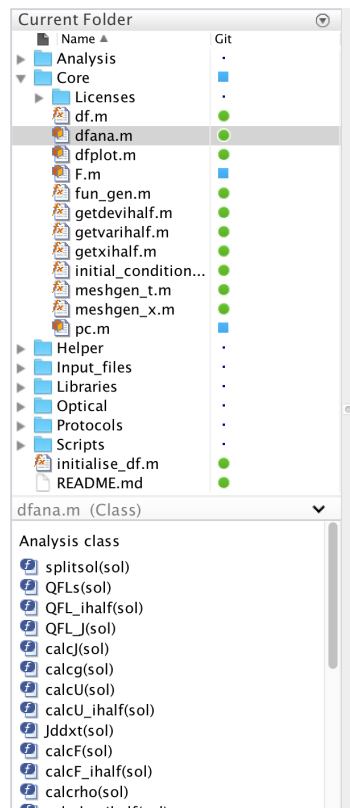


Fig. S.20 The MATLAB functions browser illustrating how to easily navigate to analysis subfunctions of **dfana**. Selecting the appropriate class in the MATLAB folder browser displays the available methods in the function browser. Double-clicking the name of the method in the function browser then navigates the user to the corresponding code.

7 Troubleshooting

We hope that your experience using Driftdiffusion, will be a relatively trouble-free experience. Along with the possibility of minor bugs that come with experimental research software, you may encounter two common error messages: spatial discretization and time integration failures.

7.1 Spatial discretization has failed

This error typically occurs for one of two reasons:

1. The point density of spatial mesh is too high: Try reducing the number of points in individual layers or using a different spatial mesh type (see `meshgen.x` for possible options).
2. The boundary conditions are not consistent with initial conditions: The initial value of a variable must be consistent with those set in the boundary conditions. If the initial or boundary conditions are changed from the default, ensure that they are consistent with one another.

7.2 Time integration failure

This error occurs when the solver cannot converge and has a number of possible solutions:

1. Reduce the `par.tmax` property to reduce the total time of the simulation.
2. Reduce the `par.MaxStepFactor` property to reduce the solver's maximum time step. Please note that this may slow down solving time considerably.
3. Use the `par.K.cation` and `par.K.anion` properties to change the ionic carrier transport to be on a similar time scale to electronic carrier transport.

Time integration errors can also occur when inconsistencies are introduced to the physical model in the simulation.

7.3 Unexpected values calculated using `dfana`

As discussed in the Main Text, owing to the computational cost of using functions external to `df` for the solving the equations, the physical model described in the Equation Editor is not coupled to that used in the analysis functions. For greater consistency an obvious change to the programming architecture would be to use centralised flux and source functions to describe the physical model, which could then be called during both the solving and analysis stages. Tests have shown however that this method comes with a significant increase in computation time owing to the large number of calls made by the solver to such functions. Hence the present method of adapting the model in both `df` and `dfana` separately, while more prone to user error, is considerably more efficient.

7.4 Bug reporting

If you find a bug with Driftdiffusion please raise an issue using the `Issues` tab on the Driftdiffusion GitHub repository page.^[2] This is the best way to ensure that other users can see which bugs have been addressed and understand how they have been fixed.

8 Known issues

8.1 Linear discretisation

Many existing drift-diffusion models use Scharfetter-Gummel finite volume discretisation scheme[6][3] to account for the exponential change in carrier density in a constant electric field. In order to take advantage of MATLAB's Partial Differential Equation Parabolic and Elliptic (PDEPE) toolbox and the ease with which transport models can be altered with it, a major trade off is the use a simplified finite element discretisation scheme for which carrier densities are assumed to change linearly between neighbouring grid points. This can be compensated for somewhat with the use of a logarithmically-spaced spatial grid and a higher density of grid points. There are however limits to the allowed point density and while the comparison simulations that use the Scharfetter-Gummel scheme (Section 4.3 of the Main Text) is generally good, the user should be aware that the use of lower point densities will increase this error. One consequences of this simplified scheme is that the currents may not always be close to zero at equilibrium. Following exploratory work at lower point densities, users are encouraged to use as high a point density as possible for obtaining the final results, especially since the solver is highly efficient. Communication with Mathworks has suggested the maximum point density is a function of various factors and therefore cannot be distilled to a single value. A degree of trial and error is therefore required on the part of the user to find the maximum allowed point density for a given device configuration.

8.2 Normalisation of the dielectric constant

As may be noted from the Equation Editor (Listing 1, Main Text) the dielectric constant must be normalised for the electrostatic potential flux and source terms to avoid a spatial discretisation error. The origin of this problem is currently unknown as normalisation has little effect on the magnitude of the input values.

8.3 High extraction coefficients do not result in constant charge density at the boundaries

Under some less common operating conditions e.g. large preconditioning voltages, the carrier densities at the boundaries do not tend to their limiting value when using high extraction coefficients. Under most circumstances this can be solved by switching to fixed carrier densities at the boundaries. This does however present a problem when calculating currents for a single carrier device as the minority carrier fluxes can no longer be used as the boundary value for the fluxes. This issues is currently ongoing and under investigation.

8.4 Drift and diffusion currents do not sum to give the total current

Drift and diffusion currents calculated using `dfana.Jddxt` do not sum to give the correct current. This is related to the way in which fluxes are calculated in the solver but a solution has yet to present itself. Total carrier currents are correctly calculated using the continuity equations in `dfana.calcJ` and users are recommended to use this method instead, reserving `dfana.Jddxt` only for individual analysis of the approximate drift and diffusion currents.

References

1. Calado P (2017) Transient optoelectronic characterisation and simulation of perovskite solar cells. PhD thesis, Imperial College London, URL <https://spiral.imperial.ac.uk:8443/handle/10044/1/66894>
2. Calado P, Barnes PRF, Gelmetti I, Azzouzi M, Hilton B (2017) Driftdiffusion. URL <https://github.com/barnesgroupICL/Driftdiffusion>
3. Farrell P, Rotundo N, Doan DH, Kantner M, Fuhrmann J, Koprucki T (2016) Numerical methods for drift-diffusion models. Tech. rep., Leibniz-Institut im Forschungsverbund Berlin, Berlin
4. Nelson J (2003) The physics of solar cells. Imperial College Press
5. NREL (2017) Reference Solar Spectral Irradiance: ASTM G-173. URL <http://rredc.nrel.gov/solar/spectra/am1.5/ASTMG173/ASTMG173.html>
6. Scharfetter DL, Gummel HK (1969) Large-Signal Analysis of a Silicon Read Diode Oscillator. IEEE Transactions on Electron Devices ED-16(1)
7. Shuttle CG (2008) Recombination dynamics in polythiophene: fullerene solar cells. PhD thesis, Imperial College London